RSC Advances

REVIEW

View Article Online
View Journal | View Issue

Cite this: *RSC Adv.*, 2026, **16**, 13223

Advances in NP shapes and their applications in cancer therapy

Xiaoqian Li,[a] Junqing Li,[a] Yimer Seid Ali,[a] Jianjun Ji,[b] Xiaohong Wen,[a] Fang Wu[c] and Chuanpin Chen *[a]

Cancer is a major global cause of death, yet traditional treatments such as surgery, chemotherapy, and radiotherapy have inherent limitations. Nanoparticles (NPs) are rapidly emerging as drug delivery systems for cancer treatments, offering promising advancements to overcome associated challenges and enhance therapies. Innovation in nanoparticle shapes is crucial in nanotechnology research worldwide. Studies indicate that the shape of nanoparticles can affect their tumor-targeting efficiency and blood circulation time. For example, the tumor accumulation of nanorods is reported to be 3–5-times higher than that of nanospheres, while the blood circulation time of nanodisks can be extended by 2–3-times compared to nanospheres. In this review, we first introduce different shapes of nanoparticles, illustrate their fabrication processes, and present their applications. Then, we examine recent research on NP shapes for various cancer treatments, discussing their challenges, perspectives, and potential impact on oncology and offering a deeper understanding.

Received 30th November 2025
Accepted 29th December 2025

DOI: 10.1039/d5ra09247g

rsc.li/rsc-advances

1. Introduction

Cancer is one of the leading causes of death globally.[1,2] However, conventional treatment methods, such as chemotherapy, are often limited by nonspecific targeting and high systemic toxicity.[3–6] To address these challenges, nanomedicine has emerged as a promising field, utilizing the knowledge and technique of nanoscience to enhance the diagnosis, prevention, and treatment of diseases.[7–9]

As fundamental carriers in nanomedicine, nanoparticles offer multiple advantages for cancer therapy. They can be loaded with drugs and passively target tumors through the enhanced permeability and retention (EPR) effect, reducing off-target effects.[10–15] Furthermore, they can be engineered as stimuli-responsive systems (*e.g.*, responsive to pH, light, and ultrasound) for controlled drug release at tumor sites.[16–21] Beyond drug delivery, the inherent optical, magnetic, and thermal properties of nanoparticles enable novel therapeutic modalities such as photothermal therapy (PTT), sonodynamic therapy (SDT), and radiation therapy (RT), which are non-invasive and can improve patient compliance.[22–29]

[a]*Xiangya School of Pharmaceutical Sciences, Central South University, Changsha, 410013, China. E-mail: ccpin2000@hotmail.com*
[b]*Zhejiang Provincial People's Hospital, Hangzhou, 310014, China*
[c]*Department of Gastroenterology, The First Affiliated Hospital of Wenzhou Medical University, Wenzhou, 325000, China*

Xiaoqian Li

Xiaoqian Li is currently a Master's student at the Xiangya School of Pharmaceutical Sciences, Central South University. Her current research focuses on the preparation of nanoparticles and their application in the combined treatment of triple-negative breast cancer through sonodynamic therapy and chemotherapy.

Chuanpin Chen

Chuanpin Chen is a Professor and PhD supervisor at the Xiangya School of Pharmaceutical Sciences, Central South University. His research focuses on the preparation of monodisperse micro-/nano-droplets and microspheres, the fabrication of monodisperse microbubble ultrasound contrast agents, and the application of surface-enhanced Raman spectroscopy in pharmaceutical analysis.

The size and shape of nanoparticles can affect their properties and functions greatly. In nanomedicine, nanoparticles with a size between 10 and 100 nm are the most suitable for blood circulation because they are big enough to avoid clearance by the kidneys and lymphatic vessels and small enough to avoid opsonization.[30–32] Different shapes of nanoparticles significantly impact their cytotoxicity, cell uptake, targeting ability, biocompatibility, and biodistribution, thereby affecting their cancer treatment efficiency.[33–35] To date, numerous nanoparticles with different shapes have been developed.[36–39] Nanotechnology research is focused on the innovation of anisotropic nanoparticles, as they have excellent application prospects in cancer treatment.[40–43] For example, Liu *et al.* prepared MoS_2 nanoflowers with a high photothermal conversion efficiency (PCE) for breast cancer therapy, which were proven to kill most cancer cells thoroughly.[44] Huang *et al.* developed DNA nanotubes containing RTA for cancer therapy, which effectively inhibited tumor growth upon systemic administration.[4]

The innovation in nanoparticle shapes has emerged as a pivotal frontier in nanomedicine, playing a crucial role in enhancing drug delivery efficiency, tumor targeting ability, and therapeutic efficiency. While nanospheres have dominated this field for a long time, nanoparticles with other shapes, such as nanocages, nanostars, and nanorods, have demonstrated unique advantages in cellular uptake, biodistribution, *etc.* However, the safe and effective clinical translation of these anisotropic nanoparticles remains a challenge. This review highlights recent advancements in nanoparticle shapes and the applications of nanoparticles with different shapes in cancer treatment. We believe that by bridging the gap between fundamental research and clinical applications, nanoparticles with different shapes may revolutionize oncology in the next few decades.

2. Conventional-shaped nanoparticles

2.1 Nanospheres

2.1.1 Characteristics and synthesis strategies. Nanospheres, characterized by their isotropic morphology, uniform physicochemical properties, excellent biocompatibility, and controllable size distribution, represent one of the earliest developed and most widely used platforms in the field of nanomedicine. They are typically synthesized through self-assembly methods, where molecules assemble into nanospheres through hydrophobic and electrostatic forces. Besides, emulsification-solvent evaporation and nanoprecipitation are suitable for the preparation of polymer nanospheres. Some other preparation methods are also available, for example, the use of a microfluidic system (for uniform nanospheres), the sol–gel method (for silicon dioxide and metal oxide nanospheres), the chemical reduction method (for metal nanospheres), and the template method (for hollow, core–shell, and porous nanospheres).

2.1.2 Drug delivery carriers. In drug delivery applications, the design of nanospheres focuses on balancing high drug loading capacity (LC), excellent biocompatibility, and controlled release behavior. Current research primarily advances along two material directions: biomacromolecular nanospheres and inorganic/organic-inorganic hybrid nanospheres.

Biomacromolecular nanospheres (*e.g.*, DNA, RNA, and proteins) offer common advantages such as superior biocompatibility, programmability, and rich biological functionalities. For example, Yang *et al.* prepared mRNA-responsive DNA nanospheres to deliver doxorubicin (DOX), which could improve the therapeutic effects of DOX by overcoming the efflux action of drug-resistant cells.[45] Song *et al.* prepared DNA-protein hybrid nanospheres to deliver DOX, which had a high drug LC and could achieve slow drug release.[46] Lu *et al.* prepared mRNA nanospheres to deliver DOX with a high drug LC of 8.2%, which exhibited a synergistic gene-chemotherapy effect in breast cancer-bearing mice (Fig. 1A).[47] However, these nanospheres commonly face challenges including scalable production, poor *in vivo* stability, and relatively complex synthesis and characterization methods.

In contrast, inorganic/organic-inorganic hybrid nanospheres (*e.g.*, carbon, zinc oxide, and mesoporous bioactive glass) exhibit shared advantages including higher physicochemical stability, easily functionalized surfaces, and unique responsive properties (*e.g.*, pH-triggered degradation and ion chelation-controlled release). For example, Qiao *et al.* prepared hollow carbon nanospheres, which could efficiently deliver 482 μg of DOX and 44 μg of siRNA to cancer cells.[48] Wang *et al.* prepared pH-responsive biodegradable ZnO nanospheres (ZnO NSs) to deliver DOX, where in the acidic tumor microenvironment, the ZnO NSs could be broken down into small fragments and release DOX.[49] Sun *et al.* prepared mesoporous bioactive glass (MBG) nanospheres as drug delivery systems. Ca^{2+} in the MBG nanospheres could chelate drug molecules, thereby effectively controlling drug release and prolonging the *in vivo* half-life of the drug.[50] However, the limitations of these materials often include uncertain biodegradability, the need for rigorous long-term toxicity evaluation, and limited functional groups in some materials (*e.g.*, carbon), requiring complex surface modifications to improve their hydrophilicity and targeting.

2.1.3 PTT. As carriers for photothermal agents (PTAs), nanospheres can accumulate in tumors *via* the EPR effect, addressing the poor targeting by traditional agents and enabling efficient tumor ablation. For example, Yu *et al.* prepared naked mesoporous rhodium nanospheres (Rh MNs) with a high PCE of up to 39%, and the cure rate of pancreatic tumors was as high as to 80%.[51] Qian *et al.* prepared $AgBiS_2$ hollow nanospheres with a high PCE of up to 44.2% (Fig. 1B).[52] Furthermore, carbon-based or metal oxide nanospheres maintain a good photothermal performance while offering a high drug LC and excellent photoacoustic imaging capabilities, enabling simultaneous therapy and visual monitoring. For example, Wu *et al.* prepared mesoporous carbon nanospheres (Meso-CNs) that had superior PTT and PAI generation ability, besides, the Meso-CNs also possessed a high drug LC (35 wt%).[53] Liang *et al.* prepared oxygen-deficient molybdenum oxide (MoO_{3-x}) hybridized hyaluronic acid (HA) hollow nanospheres; in addition to inhibiting the growth of tumors *in vivo*

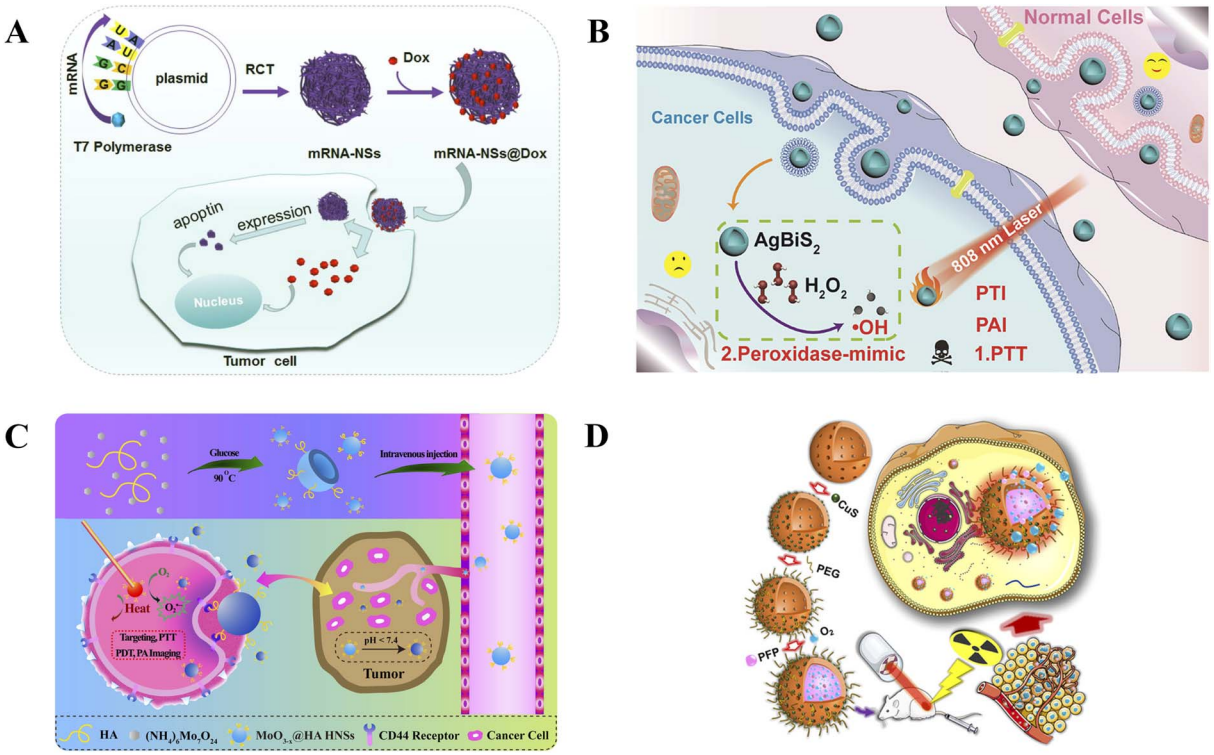

Fig. 1 (A) Schematic of the design and construction of self-assembled mRNA nanospheres and their application in chemotherapy. Reproduced with permission: copyright 2021, Elsevier.[47]. (B) Schematic showing the application of $AgBiS_2$ hollow nanospheres as PTI, PAI, and PTT agents. Reproduced with permission: copyright 2020, the American Chemical Society.[52]. (C) Schematic of the preparation of MoO_{3-x}@HA HNSs and their application in multimodal tumor phototheranostics *via* the combination of active targeting and pH responsiveness. Reproduced with permission: copyright 2018, the American Chemical Society.[54]. (D) Schematic of the design and construction of HMTCP@PFP@O_2 and its application in radiotherapy. Reproduced with permission: copyright 2019, the American Chemical Society.[57]

effectively, they could also conduct *in vivo* PAI of mice with tumors (Fig. 1C).[54]

2.1.4 RT. RT is one of the most widely used cancer treatment modalities in clinical practice. However, its therapeutic efficacy is limited by low X-ray doses and the toxicity to surrounding tissues caused by high-intensity, multi-frequency radiation beams.[55] Over the past few decades, nanospheres have garnered significant attention as tools to enhance the efficacy of radiotherapy. Their application in radio-sensitization primarily relies on the high atomic number (Z) of their constituent elements, which enables efficient X-ray absorption, generation of secondary electrons, and localized radiation dose enhancement. Various high-Z element nanospheres, such as hafnium (Hf), tantalum (Ta), tungsten (W), gadolinium (Gd), gold (Au), platinum (Pt), and bismuth (Bi), have been extensively explored. For example, Liu *et al.* prepared $W_{18}O_{49}$ nanospheres to perform RT in 4T1 tumor xenografts and realized excellent therapeutic effects.[56] Li *et al.* prepared PEGylated oxygen-carrying hollow mesoporous TaOx nanospheres modified with CuS NPs (HMTCP), which could achieve almost total inhibition of tumor growth without obvious side effects (Fig. 1D).[57] Qian *et al.* prepared $Bi_{2-x}Mn_xO_3$ nanospheres, which exhibited great potential for the treatment of 4T1 tumors *in situ* and lung metastasis.[58]

3. Container-shaped nanoparticles

3.1 Nanobowls

3.1.1 Characteristics and synthesis strategies. Nanobowls are a class of asymmetrically hollow nanostructures with a distinctive concave morphology, featuring an open cavity and a curved interior/exterior surface. Their common fabrication approaches include the template method, which is categorized into the hard template method and the soft template method. The hard template method involves first selecting a spherical template such as SiO_2 or PS nanospheres, then coating the target material onto the surface, and finally selectively etching or calcining to remove the template, resulting in a bowl-shaped structure. The only difference between the soft template method and hard template method lies in the templates, where the soft template method uses micelles or bubbles as the templates. Both the template method and emulsion interface polymerization method can be used to prepare polymer nanobowls. Apart from the above-mentioned two methods, the electrochemical deposition method is suitable for preparing metal nanobowls; 3D printing and laser ablation, as emerging methods, are suitable for fabricating high-precision nanobowls.

3.1.2 Drug delivery carriers. In the field of drug delivery, the bowl-like structure of nanobowls provides a large specific surface area, conferring a high drug LC and enabling excellent

therapeutic outcomes upon delivery to tumor sites.[59,60] For example, Luo *et al.* prepared nanobowls loaded with docetaxel (DTX) and circBNC2 (Dc-NBs), and the inhibition efficiency of tumors in the final treatment group reached approximately 90%.[61] Wang *et al.* prepared Trojan Horse-like dual-drug delivery depots that could achieve site-specific pH-near-infrared (NIR) dual-stimuli drug release, which were confirmed to effectively inhibit the growth and metastasis of tumors.[62] Furthermore, the unique rigid support offered by nanobowls allows them to function as embedded scaffolds, significantly enhancing the mechanical stability of soft carriers such as liposomes. This reinforcement helps them resist shear forces in blood flow and reduce drug leakage. For example, Fang *et al.* developed a new method to enhance the stability of actively loaded liposomal DOX by embedding a stiff nanobowl in the liposomal water cavity, which improved drug delivery to tumor sites and enhanced the antitumor efficiency (Fig. 2A).[63] These studies demonstrate that nanobowls address challenges related to targeted controlled release and circulatory stability in traditional nanocarriers through stimuli-responsive design and enhanced physical stability. However, the fabrication processes for these complex hybrid systems, along with challenges in large-scale production reproducibility and long-term *in vivo* biosafety, remain critical hurdles in their clinical translation.

3.1.3 PTT. In PTT applications, the multilayered bowl-like structure of nanobowls enables multiple internal reflections of incident light, significantly extending the optical path length and enhancing light absorption, thereby improving the PCE. For example, Liang *et al.* developed a sulfur doping strategy to synthesize sub-1 nm NiFe hydroxide ultrathin nanosheets (S–NiFe HUNs) with multilayered nanobowl-like structures. They exhibited a PCE of 29.21% and could greatly inhibit tumor growth and prolong the survival rate in a mouse model of breast cancer (Fig. 2B).[64] This case highlights the unique advantage of nanobowls in optical management, achieving localized energy concentration through structural design.

3.1.4 SDT. In the field of SDT, the asymmetric bowl-shaped morphology of nanobowls extends beyond their role as simple carriers for sonosensitizers, demonstrating active physical field modulation capabilities. Their advantages can be summarized as follows: firstly, their unconventional morphology may enhance tumor accumulation and retention; secondly, their asymmetric structure can generate a driving force under an ultrasonic field, promoting their distribution within tumor tissue; thirdly and crucially, their concave cavities can effectively trap and stabilize oxygen microbubbles generated during SDT, preventing gas dissipation, increasing the number of cavitation nuclei, and prolonging the cavitation activity duration, thereby significantly enhancing the acoustic cavitation effect and therapeutic outcomes. For example, Zhou *et al.* prepared nanobowls loaded with the small-molecule sonosensitizer Rose Bengal (RB), which could effectively inhibit the growth of tumors.[65] Song *et al.* prepared Au–platinum nanobowls that could effectively destroy malignant cells (Fig. 2C).[66] This underscores how nanobowls enhance therapeutic effects through the interaction of their morphology with physical fields, rather than solely through chemical loading.

3.1.5 Cancer detection. In the field of diagnostics, the value of nanobowls is fully realized, particularly when they (especially those made of Au) are assembled into highly ordered arrays. The periodic pore structure of nanobowls generates an intense localized electromagnetic field enhancement and signal uniformity, making them ideal substrates for ultra-sensitive surface-enhanced Raman scattering (SERS) detection. For example, Lu *et al.* prepared an SERS microfluid chip by utilizing Au nanobowls and hybridization chain reaction (HCR), and the SERS microfluid chip achieved a good linear response in the range of 10^{-12}–10^{-6} g mL^{-1}, with an ultralow limit of detection (LOD) for squamous cell carcinoma antigen (SCCA) (0.08 pg mL^{-1}) and cytokeratin 19 fragment antigen 21–1 (CYFRA21–1) (0.13 pg mL^{-1}) (Fig. 2D).[67] Cao *et al.* prepared a high-throughput microfluidic chip by combining Au nanobowls with HCR and catalytic hairpin assembly (CHA), which could achieve an

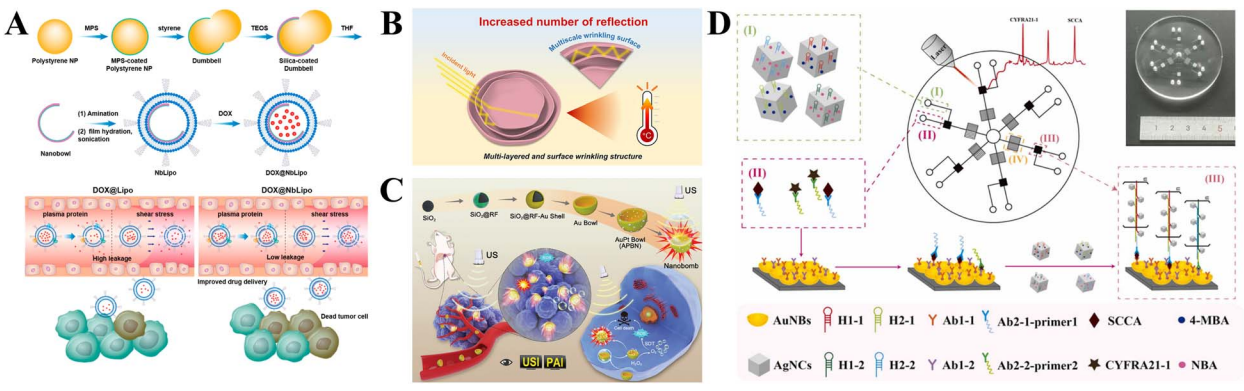

Fig. 2 (A) Schematic of the preparation of DOX@NbLipo and the effect of nanobowls in preventing DOX leakage caused by plasma protein and blood blow shear stress. (B) Mechanism of action of dS-NiFe HUNs. Reproduced with permission: copyright 2023, the American Chemical Society.[64]. (C) Schematic of the synthesis process for APBN sonosensitizers as nanobombs and their USI/PAI-guided deep orthotopic liver tumor SDT. (D) Schematic of the SERS immunoassay coupled with HCR using pump-free microfluidic chip for the detection of SCCA and CYFRA21-1. Reproduced with permission: copyright 2023, Elsevier.[67]

ultralow LOD for PIK3CA E542K (1.26 aM) and TP53 (2.04 aM), and the whole process was completed within 13 min.[68] This highlights the potential of nanobowls to transition from individual nanoparticles to ordered macroscopic functional devices.

3.2 Nanodisks

3.2.1 Characteristics and synthesis strategies. Nanodisks are flat, disk-shaped nanostructures with a diameter typically ranging from 10 to 200 nm and thickness of a few nanometers. They can be prepared *via* various methods, for example, the self-assembly method, commonly employed to prepare lipid nanodisks, involving mixing phospholipids with scaffold proteins in buffer solutions, followed by ultrasonication or thermal cycling to induce self-assembly. Alternative methods such as nanoprecipitation and film hydration method are suitable for preparing polymer nanodisks, while the hydrothermal method, template method, and lithography technique are typically employed for fabricating metal nanodisks.

3.2.2 Drug delivery carriers. In biological systems, nanodisks exhibit significant advantages due to their unique disc-like morphology. Researchers have found that red blood cell-like nanodisks can prolong the blood circulation time and enhance adhesion to vascular endothelium. Compared with spherical nanoparticles, nanodisks are more prone to lateral drift in blood flow, making them more likely to approach blood vessel walls and thereby promoting their accumulation and penetration in tumor tissues. Furthermore, the high surface-to-volume ratio of nanodisks provides a structural basis for their drug LC. Multiple studies consistently demonstrate that nanodisk systems generally exhibit a high drug LC and encapsulation efficiency (EE). For example, Shi *et al.* prepared layered double hydroxide (LDH) to load DOX, and the drug LC was as high as 34.2%.[69] Zhang *et al.* prepared biconcave carbon nanodisks with an exceedingly high drug LC (947.8 mg g^{-1}, 94.78 wt%) for DOX.[70] Li *et al.* used LAPONITE® (LP) nanodisks to deliver DOX, and the EE was as high as 80.8% ± 10.6% (Fig. 3A).[71]

In addition to their high drug LC, the morphology of nanodisks imparts intelligent stimulus-responsive drug release properties. Inspired by mammalian red blood cells, which are disc-shaped and can remain stable in high-oxygen environments while rapidly releasing oxygen in hypoxic tissues, red blood cell-like nanodisks have been designed for tumor microenvironment-responsive drug release. Yu *et al.* prepared artificial erythrocyte-like nanoparticles (RNDs), which could release DOX rapidly at tumor sites and relieve tumor hypoxia successfully.[72] This indicates that through biomimetic design, nanodisks can achieve spatiotemporally controllable functions, remaining stable during circulation in normal tissues and triggering drug release at lesion sites, thereby enhancing therapeutic specificity and reducing systemic toxicity.

3.2.3 PTT and photodynamic therapy (PDT). The high drug LC of nanodisks also makes them highly valuable for PTT and PDT. Single PTT often requires a high laser power, while single PDT relies on high doses of photosensitizers. In contrast, nanodisks can simultaneously load high concentrations of photosensitizers and integrate photothermal materials, synergistically generating cytotoxic singlet oxygen ($^1O_2$) and hyperthermia under NIR light excitation to achieve combined therapy. For example, Wang *et al.* prepared LP–PVP (LPP) composite nanodisks, and their drug LC for chlorin e6 (Ce6) was as high as 89.2% and under the excitation of an 808 nm NIR laser and 980 nm NIR laser, their PCE was 27.7% and 45.7%, respectively (Fig. 3B).[73] Conversely, metal nanodisks, by virtue of their excellent localized surface plasmon resonance (LSPR) effects, serve as efficient PTAs themselves. For example, Qiu *et al.* prepared Fe_2O_3@Au nanodisks with a high cancer cell inactivation rate of 89%.[74] Chen *et al.* prepared Bi_2Se_3 nanodisks that could effectively ablate gliomas at relatively low concentrations and inhibit tumor proliferation and migration (Fig. 3C).[75] These studies collectively highlight the flexibility of nanodisks in constructing "all-in-one" theranostic platforms, where they can function both as efficient carriers and therapeutic agents themselves.

3.3 Nanocages

3.3.1 Characteristics and synthesis strategies. Nanocages are hollow nanostructures with porous walls, typically ranging from 10 to 200 nm in diameter, featuring well-defined geometric shapes such as cubic, spherical, and octahedral. Their common preparation methods include natural protein assembly, which utilizes the self-assembly properties of ferritin or viral capsid proteins to form nanocages through pH/temperature regulation and is typically employed for fabricating protein-based or viral nanocages, respectively. In addition to the natural protein assembly method, template-directed synthesis, galvanic replacement, and solvothermal methods are typically employed for fabricating metal nanocages, while the ligand self-assembly method is utilized for metal–organic framework (MOF) nanocages and the block copolymer self-assembly method is applied for polymer nanocages.

3.3.2 Drug delivery carriers. The characteristic hollow structure and relatively large internal cavity of nanocages provide a unique physicochemical foundation for their role as efficient drug carriers. Multiple studies have confirmed that nanocages, whether carbon-based or metal-based, generally exhibit the characteristic of high LC. For example, Lei *et al.* prepared hierarchical carbon nanocages to carry the heat shock protein (Hsp70) inhibitor quercetin, and their drug LC was 60.2% (wt/wt).[76] Chen *et al.* prepared Au nanocages to carry IR-780, and their drug LC was 21.7% (Fig. 4A).[77] Sessler *et al.* prepared nanocages using lanthanide metals Eu60 and Tb60, where the LC of the Eu60 and Tb60 nanocages was 46.17% and 32.39%, respectively (in 1.5 mg mL^{-1} of DOX).[78] These findings collectively corroborate the universal advantage of hollow structures in enhancing the loading efficiency.

Among the various nanocages, ferritin nanocages are particularly favored due to their inherent biological properties. Related research has revealed the significant advantages of ferritin nanocages, as follows: (1) excellent biocompatibility and stability, which can improve the pharmacokinetic behavior of poorly soluble drugs. (2) Inherent tumor-targeting ability,

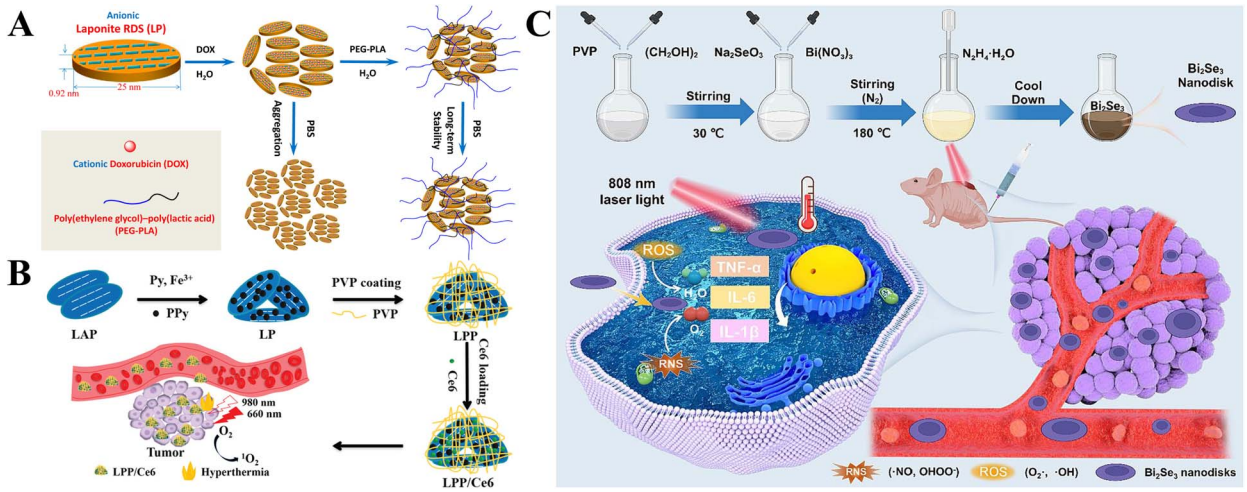

Fig. 3 (A) Schematic of the fabrication of LP/DOX (LD nanocomplexes) and LP/DOX/PEG–PLA (LDP nanohybrids) nanocarriers. Reproduced with permission: copyright 2014, the American Chemical Society.[71]. (B) Schematic of the preparation of LPP nanodisks and Ce6 loading. Reproduced with permission: copyright 2019, the American Chemical Society.[73]. (C) Schematic of the synthesis and underlying mechanisms of Bi_2Se_3 nanodisks for noninflammatory PTT. Reproduced with permission: copyright 2024, Elsevier.[75]

enabling the active targeting of tumors *via* pathways such as transferrin receptor 1 (TfR1), thereby reducing their accumulation in non-target organs. (3) Stimulus-responsive drug release, capable of triggering release in the slightly acidic tumor microenvironment, thus lowering off-target toxicity. For example, Wang *et al.* prepared H-ferritin nanocages loaded with DOX (DOX@HFn), where *in vivo* experiments confirmed that DOX@HFn can significantly inhibit tumor growth, with >30% of tumors completely eliminated.[79] In a different study, Fan *et al.* prepared ferritin nanocages (ins-FDC) to deliver camptothecin (CPT) and epirubicin (EPI), where ins-FDC showed enhanced therapeutic effects against glioma, metastatic liver cancer, and chemo-resistant breast tumors.[80] These advantages make it an ideal platform for achieving smart delivery. However, the large-scale production, batch-to-batch consistency, and

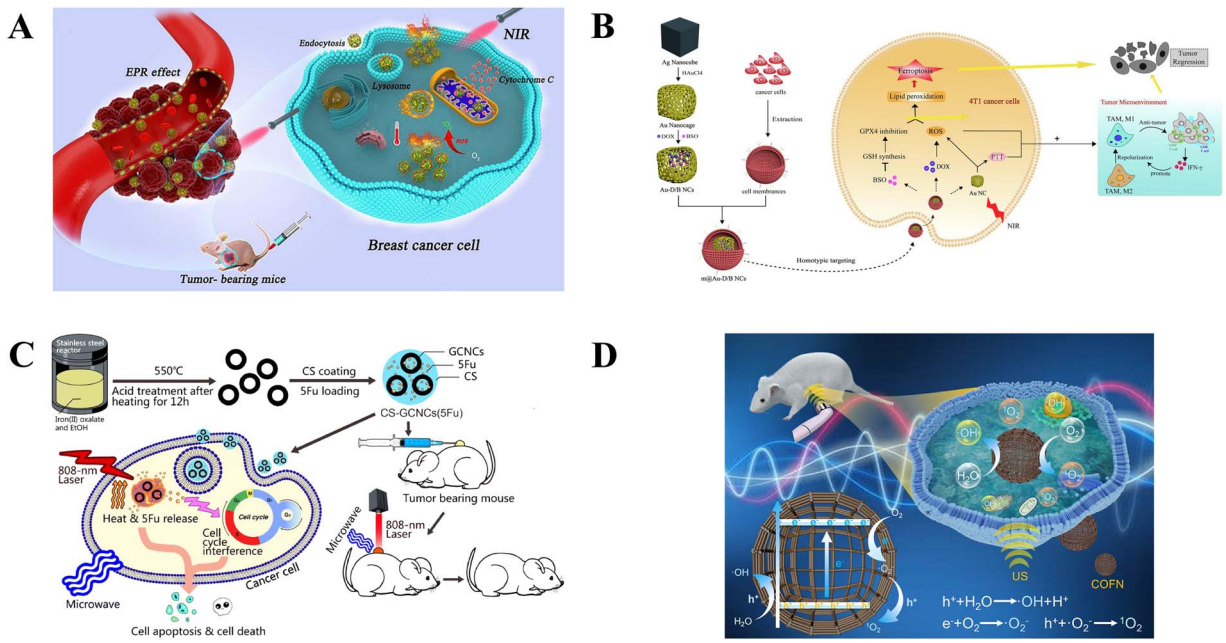

Fig. 4 (A) Schematic of the PTT strategy of AuNCs-Plu-IR780 for tumor-bearing mice. Reproduced with permission: copyright 2021, Elsevier.[77]. (B) Illustration of the formation of m@Au–C/B NCs and the mechanisms of m@Au–C/B NC-induced tumor regression. Reproduced with permission: copyright 2022, Elsevier.[83]. (C) 5Fu-loaded chitosan-coated graphitic carbon nanocages for chemo-photothermal therapy using microwave irradiation. Reproduced with permission: copyright 2020, Elsevier.[84]. (D) Schematic of SDT based on porphyrin-based COFNs. Reproduced with permission: copyright 2023, the American Chemical Society.[86]

long-term storage stability of ferritin nanocages remain practical challenges for their clinical translation.

3.3.3 PTT. In the field of PTT, Au nanocages are some of the most extensively studied systems, possessing excellent properties such as biocompatibility, specific absorption in the NIR region, and high PCE. For example, Cui *et al.* prepared Au nanocages loaded with DOX and SiRNAs, resulting in the treatment group showing a tumor inhibition ratio of more than 90% and a survival rate of 67%.[81] Chen *et al.* prepared liposomal Au nanocages (MGL), which could effectively inhibit tumor growth, recurrence, and invasion.[82] Shen *et al.* prepared cancer cell membrane-camouflaged Au nanocages loaded with DOX and L-buthionine sulfoximine (BSO) (m@Au-D/B NCs), which could significantly inhibit tumor growth without severe toxicity (Fig. 4B).[83] In comparison, graphitic carbon nanocages (GCNCs) constitute another promising platform due to their low toxicity, high drug LC, and good photothermal performance. For example, Chu *et al.* prepared GCNCs loaded with 5-fluorouracil (5FU), which exhibited strong cell-killing and tumor ablation activities (Fig. 4C).[84] In another study, the GCNCs prepared by a research group could effectively kill cancer cells and inhibit tumor growth under the irradiation power of a 980-nm laser.[85]

3.3.4 SDT. In the field of SDT, the structure of nanocages plays a different mechanistic role compared to PTT. Their porous and hollow structure facilitates enhanced gas adsorption and exchange capacity for sonosensitizers, serving as cavitation nuclei to augment the cavitation effect. Furthermore, the large surface area of nanocages provides a convenient means for regulating surface defects, thereby promoting the generation and separation of electron–hole pairs under ultrasound irradiation to enhance the SDT performance. For example, Li *et al.* prepared organic semiconductor π-conjugated covalent organic framework nanocages (COFNs), which exhibited a 64.8% increase in $^1O_2$ production relative to a core–shell-structured COF under US irradiation, and *in vivo* experimental results showed tumor suppression of 91.4% against refractory breast cancer in mice (Fig. 4D).[86] Luo *et al.* prepared Pt–CoNi LDH nanocages that could significantly enhance therapeutic efficacy against triple-negative breast cancer (TNBC).[87] This reveals the universal value of the nanocage structure in enhancing physical energy-based therapies that are not light dependent.

4. Bionic-shaped nanoparticles

4.1 Nanostars

4.1.1 Characteristics and synthesis strategies. Nanostars are anisotropic nanoparticles characterized by a central core with multiple sharp branches (typically 3–10 arms). Nanostars are commonly fabricated *via* seed-mediated growth method, where spherical Au/silver nanoparticles are first prepared as seeds and then placed in a growth solution containing $HAuCl_4$/$AgNO_3$, reducing agent (*e.g.*, ascorbic acid), or surfactant (*e.g.*, CTAB). By controlling the reduction kinetics, metal is preferentially deposited on specific crystal facets of the seeds to form nanostars. This approach is particularly suitable for synthesizing metal nanostars. In addition to the commonly employed seed-mediated growth method, the template method can be utilized for the preparation of polymer/SiO_2 nanostars.

4.1.2 Drug delivery carriers. Compared to uniformly shaped nanoparticles, the anisotropic structure of nanostars exhibits unique advantages in biological delivery. Research indicates that their sharp branched structure can more effectively promote cellular uptake, thereby increasing drug accumulation at tumor sites.[88] Furthermore, although their tissue distribution pattern *in vivo* is similar to that of nanospheres, nanostars demonstrate lower liver retention, which helps reduce the potential toxicity to normal organs and represents an important feature in terms of their biosafety.[89] These structural advantages make nanostars a promising delivery platform. For example, Lee *et al.* prepared nanostars to deliver DOX, where the drug LC and EE were 32.66% and 51.52%, respectively (Fig. 5A).[90] Besides, Cui *et al.* prepared Au nanostars loaded with IR-780, and their EE was as high as 90.4%.[91] However, the large-scale, high-reproducibility fabrication of these complex shapes remains a common bottleneck in their practical application.

4.1.3 PTT. Au nanostars have attracted significant attention as PTAs. Their advantages can be systematically summarized as follows: firstly, their sharp tips generate an extremely strong LSPR effect, which not only provides a high PCE but also creates an intense localized electric field, significantly enhancing light harvesting and the excitation of energetic charge carriers. Secondly, their optical properties (such as absorption peak and PCE) can be finely tuned by adjusting their width, length, and number of branches to match lasers of different wavelengths. Finally, the Au material itself offers good biocompatibility and an easily functionalized surface. Owing to the advantages, nanostars have garnered widespread research interest. For example, Zhao *et al.* prepared Au nanostars loaded with Ce6, which a showed high PCE (~28%) under irradiation from an 808 nm NIR laser.[92] Zhou *et al.* prepared an SERS/NIR-II optical nanoprobe comprised of Au nanostars, Raman molecular tags, and silver sulfide quantum dots through silica bridges ($AuDAg_2S$), which showed a high PCE of 67.1% at 1064 nm (Fig. 5B).[93] Jia *et al.* prepared Au nanostars loaded with ultrasmall cerium dioxide (CeO_2), myricetin (Myr) and hyaluronic acid (HA), which showed a high PCE and could achieve precise thermal ablation when exposed to light irradiation with a wavelength of 808 nm (Fig. 5C).[94] The aforementioned research highlights the high degree of design flexibility of nanostars as a multifunctional PTT platform.

4.1.4 Cancer detection. The structural characteristics of Au nanostars make them ultrasensitive contrast agents for SERS. Their multiple sharp tips act as natural "hot spots", greatly enhancing the localized electromagnetic field and thereby achieving a detection sensitivity far exceeding that of other Au nanostructures (such as nanospheres and nanorods), even down to pM levels. This property surpasses the limitations of traditional imaging techniques. For example, Bardhan *et al.* prepared immunoactive Au nanostars, which can accurately detect PD-L1 cancer cells and $CD8^+$ cells simultaneously *in vivo* by using SERS, exceeding the limitation of current immunoimaging techniques (Fig. 5D).[95] Cui *et al.* prepared Au nanostars shell-wrapped with MIL-100 (Fe), which could be used as

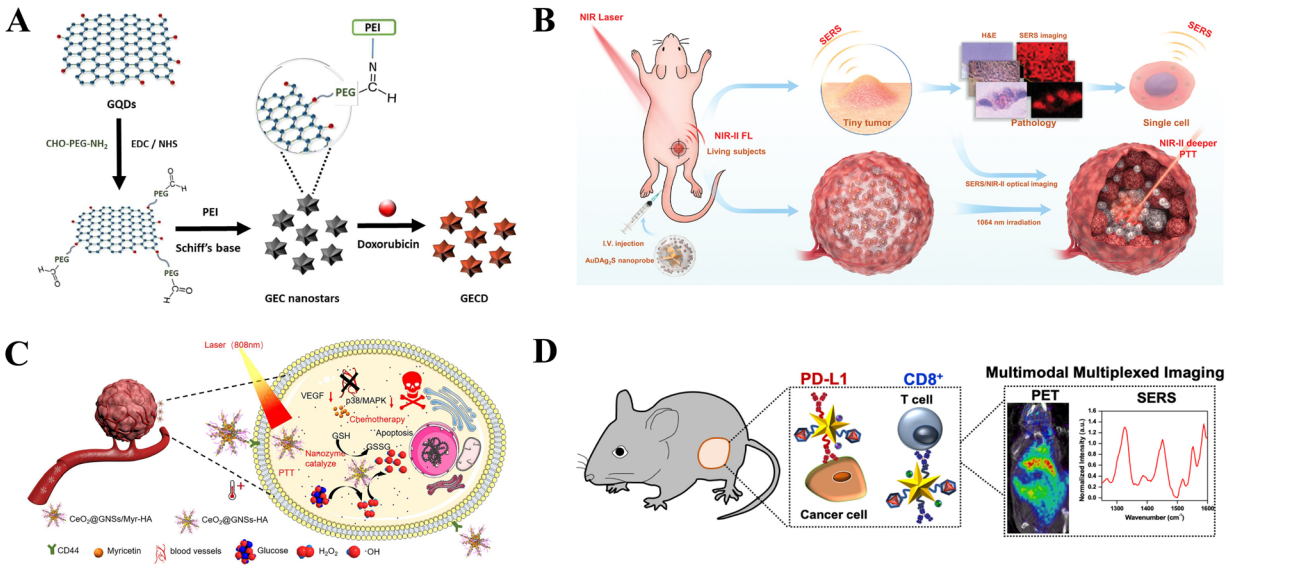

Fig. 5 (A) Synthetic process for GE, GEC, and GECD. Reproduced with permission: copyright 2022, Elsevier.[90]. (B) Schematic depicting $AuDAg_2S$ nanoprobes integrating SERS/NIR-II imaging for multidimensional tumor imaging *in vivo* (from tissue pathology to single-cell resolution) and for guiding deep-tumor NIR-II photothermal therapy. (C) Schematic of CeO_2@GNSs/Myr-HA working at the tumor site. Reproduced with permission: copyright 2025, Elsevier.[94]. (D) Schematic of the IGN-mediated multimodal multiplexed immunoPET-SERS imaging to detect both PD-L1 expression and $CD8^+$ T cells in melanoma tumors. Reproduced with permission: copyright 2019, the American Chemical Society.[95]

sensors of SERS and could selectively detect some VOCs, such as 2-butanone, eucalyptol and isopropanol.[96] This demonstrates that nanostars are not only therapeutic tools but also powerful diagnostic and sensing platforms.

4.2 Nanoflowers

4.2.1 Characteristics and synthesis strategies. Nanoflowers are three-dimensional hierarchical structures, exhibiting a flower-like morphology with a high surface area, tunable porosity (2–50 nm), and abundant active sites (typically 50–500 nm in size). The most commonly employed methods for the synthesis of nanoflowers are the hydrothermal and solvothermal methods, both involving the reaction of metal precursors with surfactants under high temperature and pressure to facilitate their self-assembly into flower-like structures. These techniques are typically used to prepare metal oxide and metal sulfide nanoflowers. Additionally, electrochemical deposition is generally applied for metallic nanoflowers, biomineralization for bioinspired nanoflowers, and one-pot rolling circle amplification for DNA nanoflowers.

4.2.2 Drug delivery carriers. The high specific surface area and internal porosity of nanoflowers generally enable them to exhibit an extremely high drug LC and EE. For example, Lu *et al.* prepared nanoflowers loaded with DOX, and the drug LC was 90.0%.[97] Du *et al.* prepared DNA nanoflowers to deliver DOX, with the drug LC reaching 73.24% ± 3.45%.[98] Yang *et al.* prepared nanoflowers with a drug LC for DOX of 69.21% (Fig. 6A).[99] However, balancing a high drug LC with controlled release and ensuring the long-term stability of these complex structures in physiological environments remain common bottlenecks in their practical application.

4.2.3 PTT. The unique flower-like hierarchical structure of nanoflowers significantly enhances their ability to capture and absorb incident light due to their rough surfaces and multi-level porosity, which greatly increases their specific surface area. This structural feature generally results in a higher PCE compared to nanoparticles with simple geometries such as spheres or rhomboids, making nanoflowers highly attractive for PTT applications. For example, Lin *et al.* prepared MoS_2 nanoflowers that possessed a high PCE and photothermal stability under irradiation from an 808 nm NIR laser.[100] In another study, Ai *et al.* prepared a high-density cuprous-supported MoS_2 nanoflower platform, which exhibited a high PCE value of 45.44% (Fig. 6B).[101] This highlights how composite structural design can further enhance the photothermal performance.

4.2.4 SDT. The large specific surface area and abundant active sites of nanoflowers also make them highly efficient sonosensitizer platforms, well-suited for SDT. Their hierarchical porous structure facilitates cavitation effects in acoustic fields and provides numerous catalytic sites, enabling the efficient generation of cytotoxic reactive oxygen species (ROS) under ultrasound activation to kill cancer cells. Studies have confirmed that nanoflowers of different compositions can leverage this structural advantage to enhance the SDT efficacy. For example, Liu *et al.* prepared molybdenum disulfide nanoflowers (MoS_2 NF), which have a high efficiency of ROS generation (Fig. 6C).[102] Xue *et al.* prepared $CoFe_2O_4$ nanoflowers, which could effectively promote the generation of ROS.[103] These findings collectively indicate that the structural characteristics of nanoflowers are a key factor in improving their SDT therapeutic outcomes.

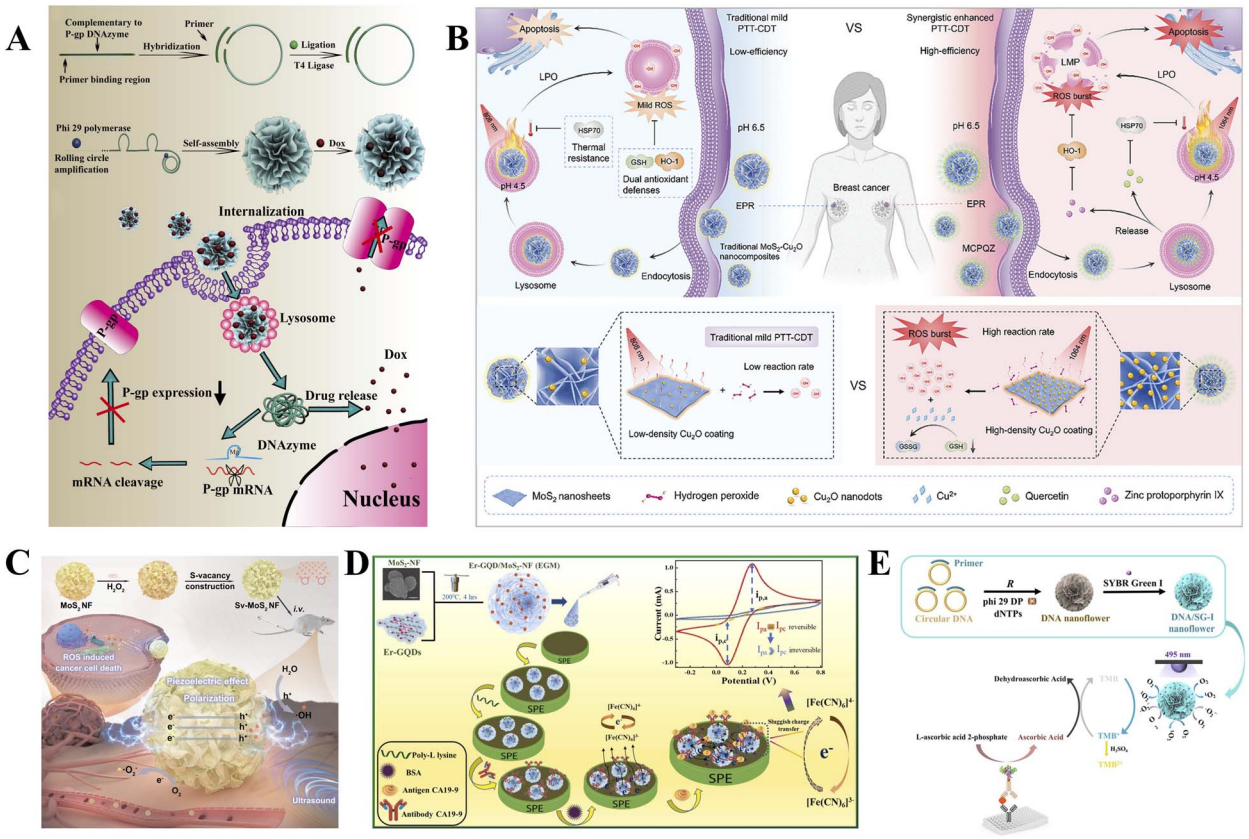

Fig. 6 (A) Sequence-independent self-assembly of the P-gp DNAzyme NFs and the mechanism of DNAzyme NFs for reversing tumor multidrug resistance. Reproduced with permission: copyright 2022, Elsevier.[99] (B) Schematic of the anticancer mechanism of the MCPQZ-mediated synergistic photothermal-chemodynamic therapy (PTT-CDT). (C) Schematic of the vacancy-modulated piezoelectric sonodynamic therapy. (D) Schematic of the step-by-step fabrication of the SPE||EGM/Ab immunosensor and the electrochemical detection of CA19-9 antigen. Reproduced with permission: copyright 2024, Elsevier.[104] (E) Synthetic scheme of photocatalytic DSNF and the detection of CEAs. Reproduced with permission: copyright 2025, the American Chemical Society.[106]

4.2.5 Cancer detection. The application of nanoflowers in biosensing primarily benefits from their large specific surface area and readily functionalized active sites, which provide an ideal platform for capturing target molecules and amplifying signals. For example, Doong *et al.* prepared MoS_2 nanoflowers with an LOD of (0.18–2.95) $\times$ 10^{-4} U mL^{-1} (Fig. 6D).[104] Wang *et al.* prepared Fe_3O_4@MnO_2 nanoflowers to detect pancreatic cancer exosomes with a detection limit down to 19.1 particles per mL, which is the most sensitive protocol reported thus far.[105] Notably, DNA nanoflowers demonstrate unique advantages in sensing due to their inherent biocompatibility, excellent resistance to degradation, and good solubility. For example, Wei *et al.* prepared photocatalytic DNA/SYBR Green I (SG-I) nanoflowers (DSNF), which achieved the sensitive and low-cost quantitative detection of CEA in the linear range of 0.5–80.0 ng mL^{-1}, and their LOD was 0.5 ng mL^{-1} (Fig. 6E).[106] Hong *et al.* prepared DNA nanoflowers encapsulating glucose oxidase and horseradish peroxidase (GHDFs) to detect human papillomavirus (HPV) DNA. The detection limit was 3.76 fM, the linearity range was 10 fM-1 nM, and the detection time was 25 min.[107] This demonstrates that nanoflowers can serve not only as passive carriers but also as active, intelligent diagnostic tools by integrating recognition elements and signal amplification modules.

5. Strip-shaped nanoparticles

5.1 Nanorods

5.1.1 Characteristics and synthesis strategies. Nanorods are nanomaterials characterized by a high aspect ratio, where their length is significantly greater than their diameter (typically ranging from tens of nanometers to micrometers), exhibiting a slender rod-like structure. This anisotropic morphology is a defining feature that distinguishes them from spherical or cubic nanoparticles. Metal nanorods are typically prepared *via* the electrochemical deposition method, where metal ions are reduced and grow along specific directions on the electrode surface under an electric field. Additionally, the hydrothermal method is commonly used for metal oxide nanorods, seed-mediated growth method for gold nanorods, and template and metal-assisted chemical etching method for silicon nanorods.

5.1.2 Drug delivery carriers. The high aspect ratio structure of nanorods imparts unique advantages in drug delivery.

Compared to nanospheres with a low aspect ratio, nanorods possess a larger effective contact area and a distinct geometric profile, which facilitate more efficient interaction with cell membranes, thereby promoting cellular uptake.[108,109] Professor Mitragotri's team confirmed through static cell cultures, microfluidics, mathematical models, and *in vivo* studies in mice that rod-shaped nanoparticles showed greater avidity and selectivity with endothelium, better targeting ability to tumors, and larger accumulation in tumor sites compared to spherical nanoparticles.[110] This finding reveals the potential of shape itself as an active targeting strategy.

Further studies have expanded upon this advantage through advanced materials engineering. Chen *et al.* developed mesoporous silica nanorods (MSNRs), which demonstrated a superior specific surface area and transmembrane transport rate relative to spherical nanoparticles (Fig. 7A).[111] Yu *et al.* further enhanced this system by coating MSNRs with colorectal cancer (CRC) cell membranes, achieving a 5.6-fold increase in drug accumulation within the cell nucleus.[112] However, the high aspect ratio structure may also pose potential challenges, such as difficulties in alignment within complex biological fluids and a propensity for non-specific adhesion. The quantitative relationship between aspect ratio and *in vivo* circulation behavior remains an area requiring further investigation.

5.1.3 PTT. In the field of PTT, Au nanorods have emerged as a research focus due to their exceptional properties. Their advantage stems from the ability to precisely tune their strong absorption peak to the NIR biological window, enabling effective photothermal treatment of deep-seated tissues. Additionally, Au nanorods exhibit good biocompatibility and a readily functionalized surface.[113,114] Related research demonstrates the evolution of Au nanorods from simple PTAs to multifunctional therapeutic platforms. For example, Ren *et al.* prepared Au nanorods modified with cRGD-peptide to deliver paclitaxel (PTX) and curcumin (CUR). Under laser irradiation at 0.7 W cm^{-2} for 5 min, the temperature of the nanorods could reach 45 °C and they could inhibit tumor growth.[115] Zhu *et al.* designed a nanoplatform by coating Au nanorods with degradable mesoporous silica, which could lead to efficient antitumor effects *in vitro* and *in vivo* (Fig. 7B).[116] These findings indicate that Au nanorods not only serve as efficient photothermal converters but also provide an ideal scaffold for the integration of multiple functional modules, such as targeting ligands, drug carriers, and responsive coatings, showcasing remarkable "programmability".

5.2 Nanotubes

5.2.1 Characteristics and synthesis strategies. Nanotubes are hollow, cylindrical nanostructures with diameters ranging from 0.4 to 100 nm and lengths up to micrometers or even millimeters. Their common preparation methods include chemical vapor deposition (CVD), where carbon source gases (such as methane or ethylene) decompose at high temperatures (600–1200 °C) under the catalysis of metals (*e.g.*, Fe, Co, and Ni), enabling carbon atoms to grow into nanotubes on the catalyst surface, where this method is well-suited for producing carbon nanotubes (CNTs). Additionally, the template and hydrothermal methods are effective for fabricating metal oxide nanotubes, while the self-assembly method is ideal for preparing polymer and DNA nanotubes.

5.2.2 Drug delivery carriers. The hollow structure of nanotubes not only provides a high drug LC but also, due to their unique geometry, facilitates prolonged blood circulation, enhanced accumulation and retention in tumor tissues, and promotes interaction with cell membranes, thereby improving the drug internalization efficiency. Studies have shown that compared to nanocarriers of other shapes, nanotubes can achieve equivalent therapeutic efficacy at lower drug concentrations, which helps reduce systemic toxicity.[117] For example, Lin *et al.* prepared nanotubes to load IR-780 and DOX simultaneously, and their drug LC was as high as 27.6%.[5] Kaneno *et al.* prepared PTX-loaded nanotubes and functionalized the nanotubes with antibodies for targeting prostate cancer cells. The cytotoxicity experiment showed that the above-mentioned nanotubes were more sensitive to prostate cancer and CRC cells (Fig. 8A).[118] These research findings indicate that the delivery efficacy of nanotubes stems not only from their high

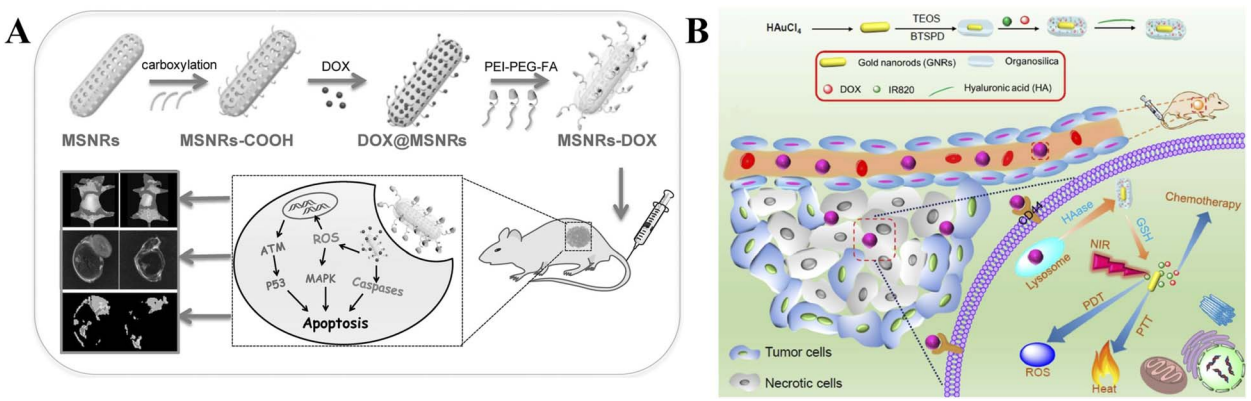

Fig. 7 (A) Rational design of the MSNR-DOX nanosystem for drug delivery and the simultaneous inhibition of cancer growth. (B) Fabrication of IR and DOX@NC with mammary adenocarcinoma-targeting, enzyme/redox-responsive release, light-activated photodynamic/thermal therapy, and chemotherapy capabilities for multi-modal tumor ablation. Reproduced with permission: copyright 2021, Elsevier.[116]

drug LC but can also be enhanced through surface functionalization, such as antibody modification, to confer active targeting capabilities, thereby helping to overcome multidrug resistance in certain tumors. However, their high aspect ratio may also lead to difficulties in degradation within the body and potential bioaccumulation. These are critical safety issues that must be systematically evaluated before their clinical translation.

5.2.3 PTT. In the field of PTT, CNTs have become a research focus due to their unique photothermal properties. The structure of CNTs, consisting of sp^2-hybridized carbon atoms arranged in rolled-up graphene sheets, endows them with efficient PCE. It is noteworthy that multi-walled carbon nanotubes (MWCNTs), owing to their greater number of absorption interfaces and superior thermal conductivity, typically exhibit more excellent heat generation efficiency compared to single-walled carbon nanotubes (SWCNTs). For example, Ming *et al.* developed MWCNTs that exhibited obvious toxicity to multidrug resistance (MDR) cancer cells under photoirradiation.[119] Zhang *et al.* prepared multi-walled carbon nanotubes-magnetofluorescent carbon quantum dot/DOX nanocomposites that could eliminate tumors effectively under NIR irradiation (Fig. 8B).[120] These results highlight that CNTs are not only efficient PTAs themselves but also possess the potential to serve as platforms for constructing multifunctional theranostic systems.

5.2.4 Cancer detection. CNTs also perform exceptionally well in the field of biosensing, primarily due to their ultra-high specific surface area, excellent electrical properties, and high sensitivity to surface adsorption. These characteristics make them ideal materials for constructing highly sensitive, label-free field-effect transistor (FET) biosensors. These sensors can achieve the highly sensitive and specific detection of various biological species, including DNA, proteins, exosomes, and even cells. For example, Zhang *et al.* developed FET-based CNTs that can detect exosomal miRNA with high sensitivity and specificity (LOD: 0.87 aM) (Fig. 8C).[121] Wei *et al.* also prepared FET-based CNTs, which could effectively discriminate prostate cancer (PCa) samples from benign prostatic hyperplasia (BPH) samples (P of 1.07×10^{-5}).[122] These studies underscore the promising application prospects of CNTs in early cancer diagnosis, liquid biopsy, and real-time monitoring, providing significant support for their evolution from therapeutic carriers to integrated "diagnosis and treatment" platforms.

5.3 Bottlebrushes

5.3.1 Characteristics and synthesis strategies. Bottlebrushes are rigid, rod-like polymers consisting of a linear backbone densely grafted with numerous side chains, exhibiting an overall cylindrical or worm-like morphology. This unique architecture, where the steric repulsion between side chains forces the backbone into an extended conformation, is the origin of their exceptional properties, such as high rigidity, reduced polymer chain entanglement, and large, accessible surface area. The common synthetic methods for bottlebrushes include the grafting-from method, grafting-to method, and macromonomer copolymerization method. Taking the grafting-to method as an example, it involves first synthesizing the backbone (containing reactive groups such as –COOH or $–NH_2$) and side chains (terminated with complementary groups such as –OH or $–N_3$) separately, followed by coupling the side chains onto the backbone *via* click chemistry (*e.g.*, CuAAC or thiol–ene reactions).

5.3.2 Drug delivery carriers. The bottlebrush architecture exhibits several systemic advantages that make it a superior drug delivery platform compared to linear or dendritic polymers. In bottlebrush polymers, which are composed of linear polymer backbones and densely grafted side chains, the densely grafted side chains create a protective "corona" that effectively shields the backbone and any conjugated payload from premature degradation and non-specific interactions, leading to enhanced stability, positive blood circulation half-life, and drug penetration into tumor tissues. In addition to the above-mentioned advantages, bottlebrush polymers are highly effective drug delivery platforms due to their enhanced solubility, improved bioavailability, controlled release behavior, and low toxicity.[123,124] Teasdale *et al.* developed a novel biodegradable PPz-g-PGA bottlebrush polymer with a high MW and showed that the bottlebrush polymer had a higher blood circulation half-life compared with linear PGA.[125]

Furthermore, the precisely tunable hydrodynamic size and rigid, extended rod-like morphology of bottlebrush polymers are ideally suited to leverage the EPR effect in solid tumors, promoting their efficient accumulation within tumor tissues.

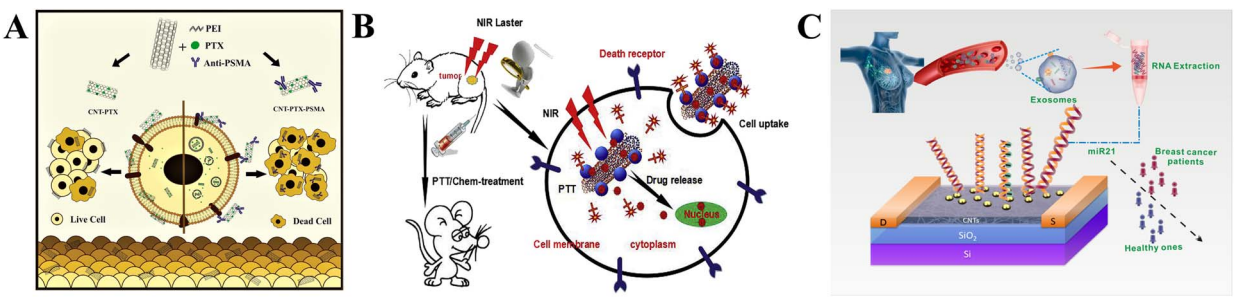

Fig. 8 (A) Schematic of the design and construction of CNTs and their use in the chemotherapy of cancers. (B) Mechanism action of CNTs *in vivo*. Reproduced with permission: copyright 2017, Elsevier.[120]. (C) Schematic of the ultrasensitive detection of exosomal miR21 using the DNA-functionalized CNT FET biosensor. Reproduced with permission: copyright 2021, the American Chemical Society.[121]

This "synergistic regulation of size and shape" forms the structural basis for their excellent *in vivo* distribution behavior. A high drug LC can be achieved through both chemical conjugation to the backbone and physical encapsulation within the hydrophobic core of amphiphilic structures, providing flexibility for co-delivery strategies. More importantly, the highly modifiable backbone and side chain termini allow for the incorporation of intelligent linkages sensitive to the tumor microenvironment (*e.g.*, acidic pH and specific enzymes). For example, Zhang *et al.* designed a biohybrid involving bottlebrush-architectured poly(ethylene glycol) (PEG) and MEL (pacMEL), which showed an ~10-fold increase in the area under the curve (AUC∞) compared with free MEL (Fig. 9A).[126] The high drug LC, achievable through both backbone conjugation and encapsulation within the hydrophobic core of amphiphilic bottlebrushes, is another critical feature. *In vivo* experiments using a poly(methacryloyloxyethyl phosphorylcholine) (pMPC)-grafted molecular bottlebrush (PCMB) conjugated with DOX through an acid-cleavable hydrazone bond demonstrated a high accumulation of DOX in tumor tissues due to the EPR effect and subsequent rapid drug release in the acidic tumor microenvironment, leading to potent antitumor activity (Fig. 9B).[127] Collectively, these studies reveal how bottlebrush platforms enable precise control over the delivery, distribution, and release of drugs through the integration of chemical design and physical structure.

5.4 Nanofibers

5.4.1 Characteristics and synthesis strategies. Nanofibers are ultrafine fibers with diameters typically ranging from 1 to 1000 nm, characterized by their high surface area-to-volume ratio, porosity, and tunable morphologies (*e.g.*, smooth, beaded, hollow, and core–shell structures). Common methods for preparing nanofibers include electrospinning, solution blow spinning, and self-assembly. The first two methods are suitable for producing polymer nanofibers, while self-assembly is typically used to prepare protein, DNA, and peptide nanofibers. Taking electrospinning as an example, it involves stretching a polymer solution or melt in a high-voltage electrostatic field, where the solvent evaporates to form nanofibers.

5.4.2 Drug delivery carriers. In the field of drug delivery, the advantages of nanofibers extend beyond merely high LC, manifesting in their unique drug-loading modalities and spatiotemporally controllable release kinetics. On one hand, as a carrier-free system, drug molecules can be directly integrated into their fibrous matrix, avoiding the potential lipid toxicity and cellular dysfunction associated with traditional nanocarriers (*e.g.*, liposomes), while achieving an exceptionally high drug LC and EE. For example, Yang *et al.* prepared supramolecular nanofibers with a high drug LC (>30 wt%) (Fig. 10A).[128] Sahin *et al.* developed nanofibers to load amygdalin (AMG) and bitter almond kernel extract, which achieved an EE of 100% ± 0.01% and 94% ± 0.02%, respectively.[129] On the other hand, the combination of their large surface area and degradability enables sustained drug release. As demonstrated by Isaei *et al.*, this can limit the initial burst release, thereby achieving better sustainability, which is crucial for maintaining stable blood drug concentrations (Fig. 10B).[130] Haririan *et al.* developed nanofibers to load temozolomide (TMZ), achieving sustained TMZ release for 30 days using the zero-order kinetic model.[131] More ingeniously, researchers have significantly enhanced the circulatory stability and therapeutic efficacy of composite systems by embedding or coating liposomes within or on nanofibers. For example, Irani *et al.* designed a PTX-loaded liposome and then incorporated the liposome into nanofibers, which showed sustained delivery of antitumor drugs (Fig. 10C).[132] Parthasarathy *et al.* successfully incorporated liposome-loaded irinotecan into nanofibers for leukemia cancer therapy, releasing it in a controlled manner over 30 days.[133] This synergistic strategy cleverly combines the high biocompatibility of liposomes with the stable and sustained-release characteristics of nanofibers.

5.4.3 PTT and PDT. As excellent carriers and dispersion matrices for high-performance photosensitizers or PTAs, nanofibers also play a pivotal role in novel therapeutic modalities such as PTT and PDT. For example, Han *et al.* successfully synthesized $CaTiO_3$: Yb, Er (CTO) nanofibers co-conjugated with RB and Au nanorods, which offered the potential for combined upconversion photoluminescence (UCPL) and enhanced synergistic PTT and PDT.[134] Lian *et al.* constructed electrospun nanofibers composed of poly(lactic acid) (PLA), poly(ε-caprolactone) (PCL) and gel, loaded with the biodegradable and high-efficiency photothermal conversion agent Prussian blue (PB), and this system demonstrated potent antitumor efficacy in

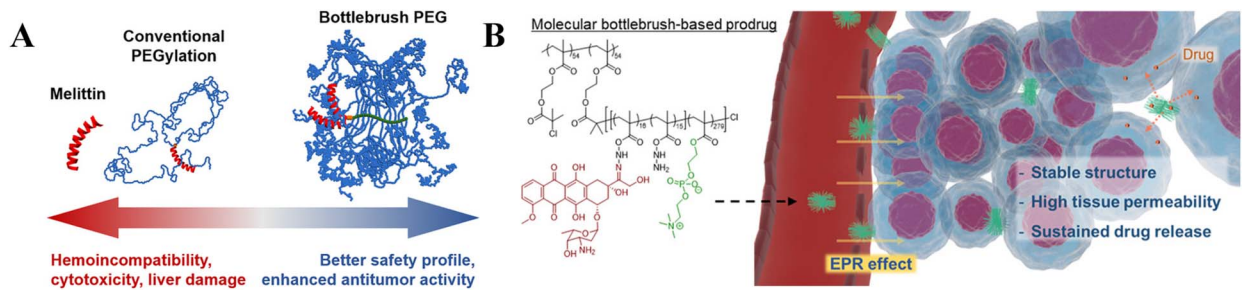

Fig. 9 (A) Description of the properties bottlebrushes. Reproduced with permission: copyright 2021, the American Chemical Society.[126]. (B) Schematic of the design and mechanism action of bottlebrushes. Reproduced with permission: copyright 2020, the American Chemical Society.[127]

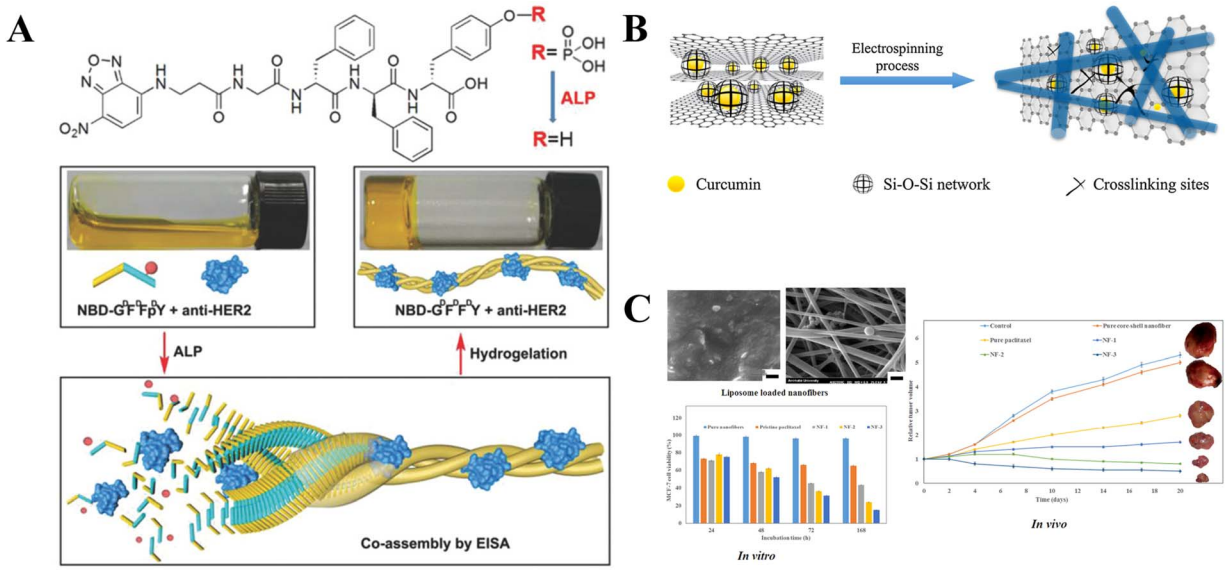

Fig. 10 (A) Chemical structures of peptides, the resulting hydrogel formed by ALP, and schematic of co-assembly between the peptide and affibody triggered by ALP (1 U mL^{-1}) at 4 °C. (B) Electrospinning process for fGO-Si-CUR containing nanofibers. Reproduced with permission: copyright 2017, Elsevier.[130]. (C) TEM images and *in vitro* and *in vivo* effects of nanofibers. Scale bar: 500 nm (TEM image on the left) and 5 μm (TEM image on the right). Reproduced with permission: copyright 2023, Elsevier.[132]

a B16 tumor-bearing mouse model.[135] This highlights the unique advantage of nanofibers in constructing an "all-in-one" multifunctional therapeutic system, *i.e.*, a versatile platform that integrates diagnostic imaging, drug delivery, and multiple treatment modalities.

6. 2D nanoparticles

6.1 Nanosheets

6.1.1 Characteristics and synthesis strategies. Nanosheets are ultra-thin two-dimensional nanoparticles with thicknesses typically below 100 nm and lateral dimensions significantly larger than their thickness, offering diverse shapes (*e.g.*, hexagonal and irregular). This class of materials encompasses graphene, transition metal dichalcogenides, black phosphorus, and LDH, among others. Their common feature of two-dimensional confinement gives rise to unique electronic, optical, and mechanical properties, forming the foundation for biomedical applications. The common methods for preparing nanosheets include liquid-phase exfoliation, chemical exfoliation, and hydrothermal method, which are typically used to produce metallic nanosheets. Taking liquid-phase exfoliation as an example, it involves first dispersing the material in a solvent, followed by exfoliation through ultrasonication or shear forces (*e.g.*, NMP solvent exfoliation of graphene) to form nanosheets.

6.1.2 Drug delivery carriers. In the field of drug delivery, the advantages of nanosheets extend far beyond the high drug LC afforded by their large specific surface area. Their two-dimensional planes and interlayer spaces collectively constitute a multimodal, intelligent drug-loading system. On one hand, their planar surfaces can load substantial amounts of drugs through physical adsorption or chemical bonding. On the other hand, the interlayer spaces of many nanosheets (*e.g.*, LDH) allow for ion exchange or molecular intercalation, enabling even higher loading rates. For example, Duan *et al.* prepared Gd_3^+-doped monolayered-double-hydroxide (MLDH) nanosheets to co-load DOX and indocyanine green (ICG), achieving an ultrahigh drug LC of 97.36% and an EE of 99.67%.[136] Guo *et al.* developed black phosphorus (BP) nanosheets that load high amounts of DOX on the sheet surface (950% by weight).[137] Zhai *et al.* prepared molybdenum oxide (MoOx) nanosheets to load DOX with a drug LC as high as 65% (Fig. 11A).[138] This reveals a key common advantage of nanosheets as a delivery platform, where their structure simultaneously provides a vast "surface reservoir" and a precisely tunable "interlayer reservoir", achieving an excellent drug LC.

6.1.3 PTT. In the field of PTT, the two-dimensional planar structure of nanosheets plays a crucial role, providing an efficient heat conduction pathway for light energy, making them suitable for PTT and enabling a high PCE. For example, Wang *et al.* developed biomimetic ultrathin graphdiyne oxide (GDYO) nanosheets with a PCE of 60.8% (Fig. 11B).[139] In another study reported by Zhou *et al.*, ultrathin MnO_2 nanosheets achieved a PCE of 62.4%, while the ReS_2 nanosheets developed by Xu *et al.* resulted in a PCE of 79.2%.[140,141] More importantly, their easily functionalized planar surface provides an excellent platform for multifunctional integration and theranostics. Their surface can be simultaneously modified with targeting molecules, loaded with chemotherapeutic drugs, or integrated with imaging probes, thereby enabling synchronous diagnostic imaging and therapy.

6.1.4 RT. In the field of RT, the application of nanosheets primarily leverages the high-Z of their constituent elements to enhance the local radiation dose. Their ultrathin structure

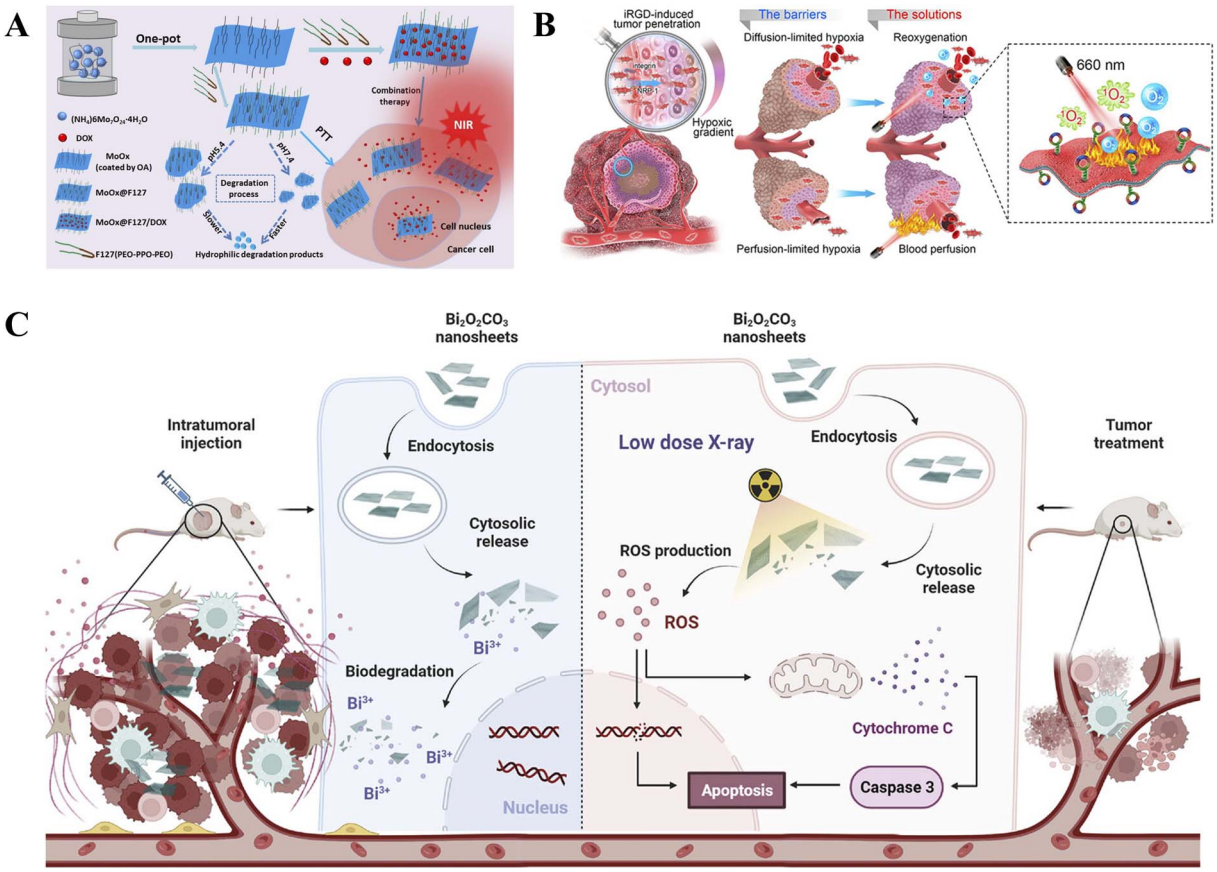

Fig. 11 (A) Schematic of the preparation, microstructure, degradation, and application of the MoOx@F127/DOX nanosheets. Reproduced with permission: copyright 2019, Elsevier.[136]. (B) Schematic of the efficient PDT ablation of tumors caused by GDYO. Reproduced with permission: copyright 2019, the American Chemical Society.[137]. (C) Schematic of the ultrathin bismuth nanosheets degrading *in vivo* and the nanosheets sensitizing tumor radiotherapy.

facilitates rapid metabolism *in vivo*, reducing the risk of long-term retention. For example, Mei *et al.* created ultrathin bismuth oxycarbonate nanosheets with a thickness of 2.8 nm using sodium oleate as a template and surface protectant, which could effectively promote cancer cell apoptosis (Fig. 11C).[142] However, their two-dimensional morphology also presents challenges. Their large planar surface may interact more readily with cell membranes, influencing their cellular internalization pathways and subcellular distribution. Furthermore, research on their *in vivo* degradation behavior and metabolic pathways remains insufficient, and addressing these issues is essential before their clinical translation can be realized.

7. Future prospects and challenges

With the rapid advancement of nanomedicine, nanoparticles of different shapes have demonstrated significant potential in cancer therapy. Compared to conventional treatments, nanomedicine offers enhanced drug delivery efficiency and reduced systemic toxicity by leveraging precise targeting, controlled release, and the EPR effect. The shape of nanoparticles serves as a critical physical parameter, profoundly influencing their blood circulation time, tumor accumulation, and cellular uptake efficiency.

However, the translation from basic research to clinical application still faces considerable challenges. Currently, only a limited number of nanoparticles with relatively simple geometries, such as spherical shapes, have entered clinical trial stages. Major bottlenecks in clinical translation include the controllable and scalable production of complex-shaped nanoparticles with batch-to-batch consistency; systematic evaluation of their *in vivo* metabolic pathways, long-term biosafety, and potential immunogenicity; as well as uncertainties in their therapeutic efficacy resulting from differences between animal models and the human tumor microenvironment.

In the future, while addressing these challenges, the rational design and optimization of nanoparticle morphology combined with stimuli-responsive materials are expected to promote more effective tumor targeting and deep tissue penetration. Further exploration of nanoparticle shapes will also contribute to the advancement of synergistic multimodal therapies, such as chemo-photothermal-immunotherapy. With progress in 3D printing, microfluidics, and computational modeling, shape control of nanoparticles is anticipated to become more precise and personalized, thereby driving their broader application in

Table 1 Drug loading types, LC/EE, and tumor models of differently shaped nanoparticles

Shape of nanoparticles	Drug	LC/EE	Tumor
Polymethacrylic acid (PMAA) nanospheres	CUR PTX	12.1%/93% 8.2%/81.6%	Breast cancer[143]
FeO–Pt@MOF nanospheres	EPI	84.1%/*	Breast cancer[144]
PEGylated oxidized mesoporous carbon nanospheres	DOX	59.7% ± 2.6%/*	Lung cancer[145]
ZnO nanospheres	DOX	24.7%/73.2%	Gastric cancer[146]
Poly(ortho ester)-disulfide polyurethane nanospheres	DOX	11.7–15.3%/61.7–71.2%	Liver cancer[147]
Eudragit s100 nanospheres	Rutin	*/94.19% ± 0.33–98.1% ± 0.5%	CRC[148]
Fe_3O_4 nanospheres	DOX	27.2%/*	Cervical cancer[149]
Oxidized mesoporous carbon nanospheres	DOX	*/86.4%	Ovarian cancer[150]
Thermosensitive dopamine nanobowls	Tirapazamine	19.6%/48.9%	Breast cancer[151]
Laponite nanodisks	DOX	*/92.1% ± 2.2%	Breast cancer[152]
VAP-PEG_{3350}-DSPE nanodisks	PTX	7.7% ± 0.34%/95.56% ± 4.52%	Lung cancer[153]
PMMA-PEG/ZnO nanodisks	CUR	92%/*	Gastric cancer[154]
Laponite nanodisks	DOX	91.5%/*	Liver cancer[155]
Laponite nanodisks	DOX	88.6% ± 1.2%/*	Ovarian cancer[156]
Mesoporous ZSM-5 zeolite/chitosan core–shell nanodisks	DOX	97.7%/*	Osteosarcoma[157]
Lipid nanodisks	Carfilzomib	8.56% ± 0.37%/93.6% ± 3.7%	Glioblastoma[158]
Chitosan/alginate nanodisks	Amoxicillin	*/74.98% ± 0.23%	Prostate cancer[159]
Lipid nanodisks	PTX	5.73% ± 0.31%/91% ± 5%	Melanoma[160]
LDH nanodisks	DOX	52.1%/*	Pancreatic cancer[69]
Silicate nanodisks	DOX	*/90%	Oral cancer[161]
Albumin nanocages	DOX	7.1%/80%	Breast cancer[162]
Au nanocages	Decitabine	84.2%/*	Liver cancer[163]
Ferritin nanocages	Mitoxantrone	9.33% ± 0.01%/90.32% ± 4.67%	CRC[164]
Au nanocages	DOX	35.81% ± 2.4%/89.54% ± 6%	Melanoma[165]
Au nanocages	5FU	*/75%	Glioma[166]
Protein nanocages	TMZ	18.7% ± 2.3%/84.3% ± 5.2%	Glioma[167]
Bi_2S_3 nanostars	DOX	13.3%/15.3%	Breast cancer[168]
Au nanostars	DOX Cisplatin	5.98%/* 7.67%/*	Liver cancer[169]
Polymer-DNA assembled nanoflowers	Dolastatin derivatives	*/85.6% ± 5%	Breast cancer[170]
DNA nanoflowers	DOX	73.24% ± 3.45%/*	Lung cancer[98]
Au nanoflowers	DOX	9.78%/62.6%	Oral cancer[171]
Mesoporous black TiO_2 nanorods	DOX	*/92%	Breast cancer[172]
Peptide nanorods	DOX	90.2%/*	Lung cancer[173]
ZnO nanorods	Daunorubicin	20.08% ± 2.36%/75.28% ± 6.43%	Liver cancer[174]
Au nanorods	Bevacizumab	45%/92%	Cervical cancer[175]
Mesoporous silica nanorods	DOX	42%/*	Nasopharyngeal carcinoma[111]
Pt/Au nanotubes	DTX	14.5%/61.6%	Breast cancer[176]
Multi-walled carbon nanotubes	DOX	25.4%/62.5%	Liver cancer[177]
Single-walled carbon nanotubes	Oxaliplatin	*/93.43% ± 1.65%	CRC[178]
Multi-walled carbon nanotubes	CUR	23.12% ± 1.22%/75.2% ± 1.17%	Melanoma[179]
Bottlebrush	DOX	48 wt%/*	Breast cancer[180]
Polymer bottlebrushes	DOX	10.2%/*	Lung cancer[181]
Amphiphilic bottlebrush copolymers	DOX	8.35%/91%	Liver cancer[182]
PCMB bottlebrushes	DOX	9.6 wt%/*	CRC[127]
Novel chitosan derivative nanofibers	CUR	*/96% ± 3.3%	Breast cancer[183]
Poly(ε-caprolactone) nanofibers	PTX	*/85%	Breast cancer[184]
PLA/PEG nanofibers	AMG	*/100% ± 0.01%	Breast cancer[129]
Poly(ε-caprolactone)-chitosan nanofibers	Capsaicin	*/98.7% ± 0.6%	Breast cancer[185]
Chitosan-poly(ethylene oxide)-poly(ε-caprolactone) nanofibers	DOX	*/74.3%	Lung cancer[186]
Poly(ε-caprolactone)/chitosan composite electrospun nanofibers	Cisplatin	*/98.6% ± 1%	Cervical cancer[187]
Electrospun chitosan/cobalt ferrite/oxidized-state nanofibers	DOX	96.5% ± 1%/*	Melanoma[188]
Coaxial electrospun nanofibers	Emodin	*/98.48% ± 0.31%	Cutaneous Malignancies[189]
MnPC nanosheets	CUR	89 wt%/*	Breast cancer[190]
FA-BSA-PEG/MoOx nanosheets	DTX	76.49%/*	Breast cancer[191]
GeP nanosheets	DOX	134 wt%/*	Liver cancer[192]
Ti_3C_2MXene nanosheets	DOX	84.2%/*	CRC[193]
PEG-CS/MMT nanosheets	DOX	26.5% ± 1.9%/88.2 ± 6.4%	Prostate cancer[194]

The * indicates that the LC or EE of the nanoparticles was not characterized in the cited references.

precision oncology. Ultimately, the optimization and development of nanoparticles with diverse shapes will not only improve the efficacy of monotherapies but also facilitate breakthroughs in multimodal combination strategies, ushering in a new era of transformative cancer treatments.

8. Conclusions

Nanomedicine demonstrates distinct advantages over conventional cancer therapies, including precise drug targeting, controlled release, EPR effect, and reduced systemic toxicity. The shape of nanoparticles serves as a key physical parameter that further optimizes their therapeutic performance, for example, nanospheres favor prolonged circulation and enhanced tumor accumulation, nanorods improve vascular extravasation and tissue penetration, while bioinspired shapes such as nanostars and nanoflowers enable multifunctional synergistic effects. This review systematically summarizes the preparation methods, biological characteristics, and applications in cancer therapy of differently shaped nanoparticles, comprehensively elucidating how their morphology influences their *in vivo* behavior and therapeutic efficacy, thereby providing an important theoretical framework and experimental guidance for further research in this field.

Looking forward, clinical translation remains a central challenge. Key issues that require urgent resolution include achieving the robust and scalable production of complex-shaped nanoparticles with batch-to-batch consistency, systematically evaluating the long-term biosafety and immunogenicity of nanoparticles with different geometries, and validating their efficacy in clinically relevant models such as drug-resistant or metastatic cancers. By overcoming these translational barriers, shape-engineered nanoparticles are poised to advance the development of truly personalized nanomedicines, ultimately enabling more precise and efficient strategies to transform cancer treatment paradigms (Table 1).

Author contributions

Xiaoqian Li: conceptualization, writing – original draft, visualization. Junqing Li: investigation, visualization, writing – review & editing. Yimer Seid Ali and Jianjun Ji: formal analysis and investigation. Xiaohong Wen: investigation and visualization. Fang Wu: conceptualization, methodology and supervision. Chuanpin Chen: conceptualization, investigation and methodology.

Conflicts of interest

There are no conflicts to declare.

Data availability

Data sharing is not applicable to this article as no data were created in this study.

Acknowledgements

This work was supported by the Natural Science Foundation of Hunan Province under Grant No. 2025JJ80076; the Joint Program on Health Science & Technology Innovation of Hainan Province under Grant No. WSJK2025MS150; the Natural Science Foundation of Hunan Province under Grant No. 2024JJ8116; and the National Natural Science Foundation of China under Grant 82370541.

References

1 Z. Zhang, J. Liu, M. Xiao, Q. Zhang, Z. Liu, M. Liu, P. Zhang and Y. Zeng, *Nano Res.*, 2022, **16**, 5206–5215.
2 X. Ji, Y. Lu, H. Tian, X. Meng, M. Wei and W. C. Cho, *Biomed. Pharmacother.*, 2019, **114**, 108800.
3 H. Li, Q. Peng, L. Yang, Y. Lin, S. Chen, Y. Qin, S. Li, X. Yu and L. Zhang, *ACS Appl. Mater. Interfaces*, 2020, **12**, 57732–57745.
4 C. H. Li, W. Y. Lv, Y. Yan, F. F. Yang, S. J. Zhen and C. Z. Huang, *Anal. Chem.*, 2021, **93**, 3526–3534.
5 E. J. Comparetti, G. G. Romagnoli, C. M. Gorgulho, V. d. A. Pedrosa and R. Kaneno, *Mater. Sci. Eng., C*, 2020, 116.
6 X. Yi, K. Yang, C. Liang, X. Zhong, P. Ning, G. Song, D. Wang, C. Ge, C. Chen, Z. Chai and Z. Liu, *Adv. Funct. Mater.*, 2015, **25**, 4689–4699.
7 S. Mehnath, K. Chitra, K. Karthikeyan and M. Jeyaraj, *Int. J. Pharm.*, 2020, 584.
8 O. C. Farokhzad and R. Langer, *ACS Nano*, 2009, **3**, 16–20.
9 Z. Cheng, M. Li, R. Dey and Y. Chen, *J. Hematol. Oncol.*, 2021, **14**, 85.
10 X. Liao, Y. Zheng, Z. Lin, Y. Shen, H. Lin, X. Liu, D. Zhang and B. Li, *Chem. Eng. J.*, 2020, **400**, 125882.
11 H. Iqbal, T. Yang, T. Li, M. Zhang, H. Ke, D. Ding, Y. Deng and H. Chen, *J. Controlled Release*, 2021, **329**, 997–1022.
12 X. Song, H. Huang, L. Xia, W. Jia, S. Yang, C. Wang and Y. Chen, *Adv. Sci.*, 2023, **10**, 2301279.
13 S. Liu, W. Li, H. Chen, J. Zhou, S. Dong, P. Zang, B. Tian, H. Ding, S. Gai, P. Yang and Y. Zhao, *ACS Nano*, 2022, **16**, 8939–8953.
14 Y. Tang, H. K. Bisoyi, X. M. Chen, Z. Liu, X. Chen, S. Zhang and Q. Li, *Adv. Mater.*, 2023, **35**, 2300232.
15 W. Wang, W. Wang, S. Jin, F. Fu, Z. Huang, Y. Huang, C. Wu and X. Pan, *Chem. Eng. J.*, 2023, **458**, 141487.
16 Y. H. Wang, K. Huang, Z. J. Qin, H. J. Xiong, T. F. Liu, T. Y. Wang, X. D. Lai, X. H. Liu, H. Jiang and X. M. Wang, *Chem. Eng. J.*, 2023, **467**, 143455.
17 H. Wu, F. Wu, T. Zhou, Z. Hu, W. Wang, X. Liang, J. Wang, C. You, B. Sun and F. Lin, *Chem. Eng. J.*, 2022, **431**, 133470.
18 N. Kong, H. Zhang, C. Feng, C. Liu, Y. Xiao, X. Zhang, L. Mei, J. S. Kim, W. Tao and X. Ji, *Nat. Commun.*, 2021, **12**, 4777.
19 H. Zhang, Z. Mao, Y. Kang, W. Zhang, L. Mei and X. Ji, *Coord. Chem. Rev.*, 2023, **475**, 214897.
20 X. Ji, Z. Tang, H. Liu, Y. Kang, L. Chen, J. Dong, W. Chen, N. Kong, W. Tao and T. Xie, *Adv. Mater.*, 2022, **35**, 2207391.

21 X. Yuan, Y. Kang, J. Dong, R. Li, J. Ye, Y. Fan, J. Han, J. Yu, G. Ni, X. Ji and D. Ming, *Nat. Commun.*, 2023, **14**, 5140.
22 D. Xia, P. Xu, X. Luo, J. Zhu, H. Gu, D. Huo and Y. Hu, *Adv. Funct. Mater.*, 2019, **29**, 1807294.
23 S. Panja, S. Maji, T. K. Maiti and S. Chattopadhyay, *ACS Appl. Mater. Interfaces*, 2015, **7**, 24229–24241.
24 D. Li, S. He, Y. Wu, J. Liu, Q. Liu, B. Chang, Q. Zhang, Z. Xiang, Y. Yuan, C. Jian, A. Yu and Z. Cheng, *Adv. Sci.*, 2019, **6**, 1902042.
25 Z. Wei, P. Liang, J. Xie, C. Song, C. Tang, Y. Wang, X. Yin, Y. Cai, W. Han and X. Dong, *Chem. Sci.*, 2019, **10**, 2778–2784.
26 H. Kang, L. Chen, Q. Li, H. Chen and L. Zhang, *ACS Appl. Mater. Interfaces*, 2023, **15**, 15129–15139.
27 F. Gong, L. Cheng, N. Yang, Y. Gong, Y. Ni, S. Bai, X. Wang, M. Chen, Q. Chen and Z. Liu, *Nat. Commun.*, 2020, **11**, 3712.
28 C. Huang, L. Zhang, Q. Guo, Y. Zuo, N. Wang, H. Wang, D. Kong, D. Zhu and L. Zhang, *Adv. Funct. Mater.*, 2021, **31**, 2010637.
29 W. Qiu, M. Liang, Y. Gao, X. Yang, X. Zhang, X. Zhang, P. Xue, Y. Kang and Z. Xu, *Theranostics*, 2021, **11**, 9652–9666.
30 L. R. MacFarlane, H. Shaikh, J. D. Garcia-Hernandez, M. Vespa, T. Fukui and I. Manners, *Nat. Rev. Mater.*, 2020, **6**, 7–26.
31 K. E. B. Doncom, L. D. Blackman, D. B. Wright, M. I. Gibson and R. K. O'Reilly, *Chem. Soc. Rev.*, 2017, **46**, 4119–4134.
32 N. E. Persson, P. H. Chu, M. McBride, M. Grover and E. Reichmanis, *Acc. Chem. Res.*, 2017, **50**, 932–942.
33 W. Jiang, Z. Zhang, M. Ye, S. Pan, G. Huang, T. Chen and X. Zhu, *Nano Today*, 2022, **46**, 101598.
34 H. Tang, H. Zhang, H. Ye and Y. Zheng, *J. Phys. Chem. B*, 2017, **122**, 171–180.
35 L. Yang, Z. Zhou, J. Song and X. Chen, *Chem. Soc. Rev.*, 2019, **48**, 5140–5176.
36 M. M. Aljumaily, N. S. Ali, A. E. Mahdi, H. M. Alayan, M. AlOmar, M. M. Hameed, B. Ismael, Q. F. Alsalhy, M. A. Alsaadi, H. S. Majdi and Z. B. Mohammed, *Water*, 2022, **14**, 1396.
37 M. Isacfranklin, F. Ameen, G. Ravi, R. Yuvakkumar, S. I. Hong, D. Velauthapillai, M. D. F. AlKahtani, M. Thambidurai and C. Dang, *Ceram. Int.*, 2020, **46**, 20553–20557.
38 T. Gao, Y. Zhang, C. Li, Y. Wang, Q. An, B. Liu, Z. Said and S. Sharma, *Sci. Rep.*, 2021, **11**, 22535.
39 M. S. Vidhya, F. Ameen, T. Dawoud, R. Yuvakkumar, G. Ravi, P. Kumar and D. Velauthapillai, *Mater. Lett.*, 2021, **283**, 128760.
40 C. Yu, X. Chen, N. Li, Y. Zhang, S. Li, J. Chen, L. Yao, K. Lin, Y. Lai and X. Deng, *Environ. Sci. Pollut. Res.*, 2022, **29**, 18423–18439.
41 F. Yu, Z. Zhu, C. Li, W. Li, R. Liang, S. Yu, Z. Xu, F. Song, Q. Ren and Z. Zhang, *Appl. Catal., B*, 2022, **314**, 121467.
42 Y. Yang, H. Zhu, X. Xu, L. Bao, Y. Wang, H. Lin and C. Zheng, *Microporous Mesoporous Mater.*, 2021, **324**, 111289.
43 Z. Zhuo, Y. Wan, D. Guan, S. Ni, L. Wang, Z. Zhang, J. Liu, C. Liang, Y. Yu, A. Lu, G. Zhang and B. T. Zhang, *Adv. Sci.*, 2020, **7**, 1903451.
44 S. Zhou, X. Jiao, Y. Jiang, Y. Zhao, P. Xue, Y. Liu and J. Liu, *Appl. Surf. Sci.*, 2021, **552**, 149498.
45 Y. Jiang, X. Xu, X. Fang, S. Cai, M. Wang, C. Xing, C. Lu and H. Yang, *Anal. Chem.*, 2020, **92**, 11779–11785.
46 D. Lee, S. Baek, Y. Y. Kim, Y. Bang, H. N. Jung, H. J. Im and Y. K. Song, *ACS Appl. Mater. Interfaces*, 2022, **14**, 37493–37503.
47 Y. Tang, X. Liao, C. Wang, Y. Liu, J. Pan, Y. Tian, Z. Teng and G. Lu, *J. Colloid Interface Sci.*, 2021, **603**, 191–198.
48 X. Du, C. Zhao, M. Zhou, T. Ma, H. Huang, M. Jaroniec, X. Zhang and S. Z. Qiao, *Small*, 2016, **13**, 1602592.
49 X. Chen, T. Niu, Y. Gao, X. Liang, S. Li, L. Zhang, L. Li, T. Wang, Z. Su and C. Wang, *Chem. Eng. J.*, 2019, **371**, 443–451.
50 B. Sui, X. Liu and J. Sun, *ACS Appl. Mater. Interfaces*, 2018, **10**, 23548–23559.
51 H. Wang, H. Wang, G. Yu, L. Xie, C. Zhang, C. Xu, X. Ma, Z. Miao and Y. Yu, *J. Colloid Interface Sci.*, 2025, **677**, 1075–1083.
52 B. Chen, C. Zhang, W. Wang, Z. Chu, Z. Zha, X. He, W. Zhou, T. Liu, H. Wang and H. Qian, *ACS Nano*, 2020, **14**, 14919–14928.
53 L. Zhou, Y. Jing, Y. Liu, Z. Liu, D. Gao, H. Chen, W. Song, T. Wang, X. Fang, W. Qin, Z. Yuan, S. Dai, Z. A. Qiao and C. Wu, *Theranostics*, 2018, **8**, 663–675.
54 Y. Y. Wang, W. L. Wang, X. C. Shen, B. Zhou, T. Chen, Z. X. Guo, C. C. Wen, B. P. Jiang and H. Liang, *ACS Appl. Mater. Interfaces*, 2018, **10**, 42088–42101.
55 Y. He, H. Chen, W. Li, L. Xu, H. Yao, Y. Cao, Z. Wang, L. Zhang, D. Wang and D. Zhou, *J. Nanobiotechnol.*, 2023, **21**, 209.
56 N. Zheng, S. Zhang, L. Wang, Z. Qi, Q. Peng, L. Jian, Y. Bai, Y. Feng, J. Shen, R. Wang, J. Jiao, W. Xu and S. Liu, *Nano Res.*, 2021, **15**, 2315–2323.
57 C. Peng, Y. Liang, Y. Chen, X. Qian, W. Luo, S. Chen, S. Zhang, Q. Dan, L. Zhang, M. Li, M. Yuan, B. Zhao and Y. Li, *ACS Appl. Mater. Interfaces*, 2019, **12**, 5520–5530.
58 B. Chen, L. Xiao, W. Wang, L. Xu, Y. Jiang, G. Zhang, L. Liu, X. Li, Y. Yu and H. Qian, *ACS Appl. Mater. Interfaces*, 2023, **15**, 33903–33915.
59 K. K. Haldar, S. Tanwar, R. Biswas, T. Sen and J. Lahtinen, *J. Colloid Interface Sci.*, 2019, **556**, 140–146.
60 A. H. Mo, P. B. Landon, K. S. Gomez, H. Kang, J. Lee, C. Zhang, W. Janetanakit, V. Sant, T. Lu, D. A. Colburn, S. Akkiraju, S. Dossou, Y. Cao, K. F. Lee, S. Varghese, G. Glinsky and R. Lal, *Nanoscale*, 2016, **8**, 11840–11850.
61 X. Pan, K. Chen, W. Gao, M. Xu, F. Meng, M. Wu, Z. Q. Wang, Y. Q. Li, W. Xu, M. Zhang and Y. Luo, *Mol. Cancer*, 2025, **24**, 29.
62 X. Chen, X. Zhang, L. Zhang, G. Zhao, S. Xu, L. Li, Z. Su, R. Liu and C. Wang, *Biomaterials*, 2021, **268**, 120541.
63 Z. J. Chen, S. C. Yang, X. L. Liu, Y. Gao, X. Dong, X. Lai, M. H. Zhu, H. Y. Feng, X. D. Zhu, Q. Lu, M. Zhao,

H. Z. Chen, J. F. Lovell and C. Fang, *Nano Lett.*, 2020, **20**, 4177–4187.
64 Y. Zhang, T. Wang, R. Hu, G. Qing, N. Gong, Y. Yang and X. J. Liang, *ACS Nano*, 2023, **17**, 20024–20033.
65 S. Zhang, S. Xia, L. Chen, Y. Chen and J. Zhou, *Adv. Sci.*, 2023, **10**, 2206009.
66 X. Lin, S. Chen, Y. Su, Y. Wu, L. Huang, Q. Ye and J. Song, *Adv. Sci.*, 2024, **11**, 2306301.
67 X. Cao, Y. Gu, Z. Li, S. Ge, Y. Mao, Y. Gu and D. Lu, *Sens. Actuators, B*, 2023, **375**, 132894.
68 X. Cao, S. Ge, W. Hua, X. Zhou, W. Lu, Y. Gu and Z. Li, *J. Nanobiotechnol.*, 2022, **20**, 271.
69 G. Li, Y. Fan, L. Lin, R. W, M. Shen and X. Shi, *Sci. China:Chem.*, 2021, **64**, 817–826.
70 Q. Mu, H. Wang, X. Gu, Z. R. Stephen, C. Yen, F. C. Chang, C. J. Dayringer and M. Zhang, *Adv. Healthcare Mater.*, 2019, **8**, 1801505.
71 G. Wang, D. Maciel, Y. Wu, J. Rodrigues, X. Shi, Y. Yuan, C. Liu, H. Tomás and Y. Li, *ACS Appl. Mater. Interfaces*, 2014, **6**, 16687–16695.
72 N. Wang, J. Li, J. Wang, D. Nie, X. Jiang, Y. Zhuo and M. Yu, *J. Controlled Release*, 2022, **350**, 886–897.
73 H. Wu, W. Wang, Z. Zhang, J. Li, J. Zhao, Y. Liu, C. Wu, M. Huang, Y. Li and S. Wang, *ACS Appl. Mater. Interfaces*, 2019, **12**, 390–399.
74 L. Li, F. Qi, J. Guo, J. Fan, W. Zheng, M. Ghulam, W. Wang, Z. Meng and L. Qiu, *J. Mater. Chem. A*, 2023, **11**, 21365–21372.
75 X. Dai, D. Liu, P. Pan, G. Liang, X. Wang and W. Chen, *J. Colloid Interface Sci.*, 2024, **661**, 930–942.
76 F. Wang, B. Wang, X. Xu, X. Wang, P. Jiang, Z. Hu, X. Wang and J. Lei, *Adv. Healthcare Mater.*, 2023, **12**, 2300834.
77 Y. Hu, S. Huang, X. Zhao, L. Chang, X. Ren, X. Mei and Z. Chen, *Chem. Eng. J.*, 2021, **421**, 129744.
78 S. Q. Wang, Y. Wang, X. Yang, Y. Liu, H. Li, Z. Yang, W. Y. Sun and J. L. Sessler, *Angew. Chem., Int. Ed.*, 2024, **63**, e202317775.
79 Y. Chen, L. Zeng, H. Zhu, Q. Wu, R. Liu, Q. Liang, B. Chen, H. Dai, K. Tang, C. Liao, Y. Huang, X. Yan, K. Fan, J. Z. Du, R. Lin and J. Wang, *Small Methods*, 2022, **7**, 2201086.
80 Z. Wang, Y. Zhao, S. Zhang, X. Chen, G. Sun, B. Zhang, B. Jiang, Y. Yang, X. Yan and K. Fan, *Theranostics*, 2022, **12**, 1800–1815.
81 Y. Yang, Y. Han, Q. Sun, J. Cheng, C. Yue, Y. Liu, J. Song, W. Jin, X. Ding, J. M. de-la-Fuente, J. Ni, X. Wang and D. Cui, *J. Nanobiotechnol.*, 2021, **19**, 54.
82 J. Li, K. Zheng, L. Lin, M. Zhang, Z. Zhang, J. Chen, S. Li, H. Yao, A. Liu, X. Lin, G. Liu and B. Chen, *Small*, 2024, **20**, 2407388.
83 Y. Wei, Z. Wang, J. Yang, R. Xu, H. Deng, S. Ma, T. Fang, J. Zhang and Q. Shen, *J. Colloid Interface Sci.*, 2022, **606**, 1950–1965.
84 Y. Guo, Y. Chen, P. Han, Y. Liu, W. Li, F. Zhu, K. Fu and M. Chu, *Acta Biomater.*, 2020, **103**, 237–246.
85 Y. Chen, Y. Guo, P. Han, D. Li, X. Gui, Z. Zhang, K. Fu and M. Chu, *Carbon*, 2018, **136**, 234–247.
86 S. Yao, Y. Zhao, Z. Wang, S. Wang, M. Zheng, Q. Hu and L. Li, *ACS Appl. Mater. Interfaces*, 2023, **15**, 34488–34496.
87 Y. Wu, Z. Zhao, M. Ma, W. Zhang, W. Liu, X. Liang, T. Zhao, Y. Luo, Y. Wang, M. Li, T. Li, C. Liu, X. Luo, S. Wang, W. Li, W. Zeng, H. Wang, W. Li, T. Wu, Z. Ke and F. Luo, *Theranostics*, 2025, **15**, 1456–1477.
88 R. Wang, N. Zhao and F. J. Xu, *Adv. Funct. Mater.*, 2017, **27**, 1700256.
89 J. Gao, M. Sanchez-Purra, H. Huang, S. Wang, Y. Chen, X. Yu, Q. Luo, K. Hamad-Schifferli and S. Liu, *Sci. China:Chem.*, 2017, **60**, 1219–1229.
90 G. Y. Lee, P. Y. Lo, E. C. Cho, J. H. Zheng, M. Li, J. H. Huang and K. C. Lee, *FlatChem*, 2022, **31**, 100320.
91 F. Xia, J. Niu, Y. Hong, C. Li, W. Cao, L. Wang, W. Hou, Y. Liu and D. Cui, *Acta Biomater.*, 2019, **89**, 289–299.
92 L. Zhang, X. Q. Yang, J. S. Wei, X. Li, H. Wang and Y. D. Zhao, *Theranostics*, 2019, **9**, 5424–5442.
93 J. He, S. Hua, D. Zhang, K. Wang, X. Chen and M. Zhou, *Adv. Funct. Mater.*, 2022, **32**, 2208028.
94 C. Li, Z. Guo, W. Jia, Y. Kang, M. Zeng, T. Gu, C. Zhou, R. Zhao, X. Cheng and N. Jia, *J. Colloid Interface Sci.*, 2025, **685**, 753–765.
95 Y. C. Ou, X. Wen, C. A. Johnson, D. Shae, O. D. Ayala, J. A. Webb, E. C. Lin, R. C. DeLapp, K. L. Boyd, A. Richmond, A. Mahadevan-Jansen, M. Rafat, J. T. Wilson, J. M. Balko, M. N. Tantawy, A. E. Vilgelm and R. Bardhan, *ACS Nano*, 2019, **14**, 651–663.
96 Y. Zhang, H. Yao, C. Xue, Y. Xu, C. Yi, Y. Sun, S. Cui, N. D. Hoa, A. Jouyban, H. Jin and D. Cui, *ACS Appl. Nano Mater.*, 2024, **7**, 2735–2743.
97 L. Ren, X. Liu, T. Ji, G. Deng, F. Liu, H. Yuan, J. Yu, J. Hu and J. Lu, *ACS Appl. Mater. Interfaces*, 2019, **11**, 45467–45478.
98 H. Liao, Y. Cao, C. Hu, S. Shen, Z. Zhang, D. Li and Y. Du, *Mater. Today Bio*, 2024, **25**, 101005.
99 L. Liang, W. Huo, B. Wang, L. Cao, H. Huo, Y. Liu, Y. Jin and X. Yang, *J. Colloid Interface Sci.*, 2022, **608**, 2985–2993.
100 B. Liu, C. Li, G. Chen, B. Liu, X. Deng, Y. Wei, J. Xia, B. Xing, P. a. Ma and J. Lin, *Adv. Sci.*, 2017, **4**, 1600540.
101 J. Huang, G. Deng, S. Wang, T. Zhao, Q. Chen, Y. Yang, Y. Yang, J. Zhang, Y. Nan, Z. Liu, K. Cao, Q. Huang and K. Ai, *Adv. Sci.*, 2023, **10**, 2302208.
102 Q. Wu, J. Zhang, X. Pan, Z. Huang, H. Zhang, J. Guo, Y. Xue, R. Shi and H. Liu, *Adv. Sci.*, 2023, **10**, 2301152.
103 S. Fu, R. Yang, J. Ren, J. Liu, L. Zhang, Z. Xu, Y. Kang and P. Xue, *ACS Nano*, 2021, **15**, 11953–11969.
104 T. V. Huynh, H. L. Tran, N. T. N. Anh and R. A. Doong, *Sens. Actuators, B*, 2024, **413**, 135893.
105 Y. Zhang, Y. Wei, P. Liu, X. Zhang, Z. Xu, X. Tan, M. Chen and J. Wang, *Anal. Chem.*, 2021, **93**, 11540–11546.
106 S. He, Y. Chen, H. Lian, X. Cao, B. Liu and X. Wei, *Anal. Chem.*, 2025, **97**, 4350–4358.
107 H. He, L. Cheng, Y. He, J. Chen, L. Song, Y. Yang, Y. Zhang, Z. Lin and G. Hong, *Sens. Actuators, B*, 2022, **371**, 925–4005.
108 S. Dasgupta, T. Auth and G. Gompper, *Nano Lett.*, 2014, **14**, 687–693.

109 C. Lee, H. S. Hwang, S. Lee, B. Kim, J. O. Kim, K. T. Oh, E. S. Lee, H. G. Choi and Y. S. Youn, *Adv. Mater.*, 2017, **29**, 935–9648.
110 P. Kolhar, A. C. Anselmo, V. Gupta, K. Pant, B. Prabhakarpandian, E. Ruoslahti and S. Mitragotri, *Proc. Natl. Acad. Sci. U. S. A.*, 2013, **110**, 10753–10758.
111 Y. You, L. He, B. Ma and T. Chen, *Adv. Funct. Mater.*, 2017, **27**, 1616–301X.
112 J. Wang, H. Pan, J. Li, D. Nie, Y. Zhuo, Y. Lv, N. Wang, H. Chen, S. Guo, Y. Gan, X. Yang and M. Yu, *Chin. Chem. Lett.*, 2023, **34**, 1001–8417.
113 S. J. Kim, H. B. Park, E. K. An, D. Ryu, W. Zhang, C. G. Pack, H. Kim, M. Kwak, W. Im, J. H. Ryu, P. C. W. Lee and J. O. Jin, *J. Controlled Release*, 2024, **373**, 105–116.
114 J. Ye, J. Yu, M. Zhao, Y. Zhang, Z. Wang, S. Li, B. Zhang, H. Zhang, T. Zhou, Y. Wang, X. Li, Z. He, H. Liu and Y. Wang, *J. Colloid Interface Sci.*, 2025, **678**, 272–282.
115 F. Zhu, G. Tan, Y. Zhong, Y. Jiang, L. Cai, Z. Yu, S. Liu and F. Ren, *J. Nanobiotechnol.*, 2019, **17**, 1477–3155.
116 D. Cheng, Y. Ji, B. Wang, Y. Wang, Y. Tang, Y. Fu, Y. Xu, X. Qian and W. Zhu, *Acta Biomater.*, 2021, **128**, 435–446.
117 J. Y. Park, G. H. Lee, K. H. Yoo and D. Khang, *J. Nanobiotechnol.*, 2023, **21**, 1477–3155.
118 X. Cai, M. Wang, P. Mu, T. Jian, D. Liu, S. Ding, Y. Luo, D. Du, Y. Song, C. L. Chen and Y. Lin, *Research*, 2021, **2021**, 2639–5274.
119 X. Suo, B. N. Eldridge, H. Zhang, C. Mao, Y. Min, Y. Sun, R. Singh and X. Ming, *ACS Appl. Mater. Interfaces*, 2018, **10**, 33464–33473.
120 M. Zhang, W. Wang, F. Wu, P. Yuan and C. Chi, *Carbon*, 2017, **123**, 70–83.
121 T. Li, Y. Liang, J. Li, Y. Yu, M. M. Xiao, W. Ni, Z. Zhang and G. J. Zhang, *Anal. Chem.*, 2021, **93**, 15501–15507.
122 W. Liu, X. Wang, B. Dong, Y. Liu and D. Wei, *Biosens. Bioelectron.*, 2024, **263**, 2155–6210.
123 H. Li, H. Liu, T. Nie, Y. Chen, Z. Wang, H. Huang, L. Liu and Y. Chen, *Biomaterials*, 2018, **178**, 620–629.
124 L. Shao, H. Zhang, L. Sun, L. Ning, X. Sun, C. Qin, W. Xu, R. Xu and F. Jia, *Adv. Healthcare Mater.*, 2025, **14**, 2192–2640.
125 P. Strasser, B. Montsch, S. Weiss, H. Sami, C. Kugler, S. Hager, H. Schueffl, R. Mader, O. Brüggemann, C. R. Kowol, M. Ogris, P. Heffeter and I. Teasdale, *Small*, 2023, **19**, 1613–6810.
126 F. Jia, P. Chen, D. Wang, Y. Sun, M. Ren, Y. Wang, X. Cao, L. Zhang, Y. Fang, X. Tan, H. Lu, J. Cai, X. Lu and K. Zhang, *ACS Appl. Mater. Interfaces*, 2021, **13**, 42533–42542.
127 S. Takano, W. Islam, K. Nakazawa, H. Maeda, K. Sakurai and S. Fujii, *Biomacromolecules*, 2020, **22**, 1186–1196.
128 C. Liang, L. Zhang, W. Zhao, L. Xu, Y. Chen, J. Long, F. Wang, L. Wang and Z. Yang, *Adv. Healthcare Mater.*, 2018, **7**, 2192–2640.
129 S. A. Seyhan, D. B. Alkaya, S. Cesur and A. Sahin, *Int. J. Biol. Macromol.*, 2023, **239**, 0141–8130.
130 R. Sedghi, A. Shaabani, Z. Mohammadi, F. Y. Samadi and E. Isaei, *Carbohydr. Polym.*, 2017, **159**, 1–10.
131 M. Irani, G. M. M. Sadeghi and I. Haririan, *Int. J. Biol. Macromol.*, 2017, **97**, 744–751.
132 K. Hasanbegloo, S. Banihashem, B. Faraji-Dizaji, S. Bybordi, N. Farrokh-Eslamlou, P. G. S. Abadi, F. S. Jazi and M. Irani, *Int. J. Biol. Macromol.*, 2023, **230**, 0141–8130.
133 C. Govindasamy, A. S. El-Newehy, S. H. Hussein-Al-Ali, P. Arulselvan, M. Bharathi and S. Parthasarathy, *Int. J. Biol. Macromol.*, 2024, **270**, 0141–8130.
134 Y. K. Fu, H. Liu, Z. H. Ren, X. Li, J. Huang, S. Best and G. R. Han, *J. Mater. Chem. B*, 2017, **5**, 2050–7518.
135 J. X. Mu, Z. X. Meng, X. R. Liu, P. Guan and H. Lian, *Adv. Fiber Mater.*, 2023, **5**, 2524–7921.
136 L. Peng, X. Mei, J. He, J. Xu, W. Zhang, R. Liang, M. Wei, D. G. Evans and X. Duan, *Adv. Mater.*, 2018, **30**, 1521–4095.
137 W. Chen, J. Ouyang, H. Liu, M. Chen, K. Zeng, J. Sheng, Z. Liu, Y. Han, L. Wang, J. Li, L. Deng, Y. N. Liu and S. Guo, *Adv. Mater.*, 2016, **29**, 1521–4095.
138 Y. Chen, A. R. Khan, D. Yu, Y. Zhai, J. Ji, Y. Shi and G. Zhai, *J. Colloid Interface Sci.*, 2019, **553**, 567–580.
139 W. Jiang, Z. Zhang, Q. Wang, J. Dou, Y. Zhao, Y. Ma, H. Liu, H. Xu and Y. Wang, *Nano Lett.*, 2019, **19**, 4060–4067.
140 L. Wang, S. Guan, Y. Weng, S. M. Xu, H. Lu, X. Meng and S. Zhou, *ACS Appl. Mater. Interfaces*, 2019, **11**, 6267–6275.
141 Z. H. Miao, L. X. Lv, K. Li, P. Y. Liu, Z. Li, H. Yang, Q. Zhao, M. Chang, L. Zhen and C. Y. Xu, *Small*, 2018, **14**, 1613–6810.
142 S. Shi, X. Li, Y. Zhang, H. Huang, J. Liu, J. Zhang, Z. Wang, H. Niu, Y. Zhang and Q. Mei, *Small*, 2024, **20**, 1613–6810.
143 M. Lu, M. Wu, Y. Huang, J. Yao, Z. Shao and X. Chen, *J. Mater. Chem. B*, 2022, **10**, 3798–3807.
144 J. Li, Y. Zhou, S. Yan, W. Wu and M. Sharifi, *Arabian J. Chem.*, 2023, **16**, 1878–5352.
145 X. Cai, H. Yan, Y. Luo, Y. Song, Y. Zhao, H. Li, D. Du and Y. Lin, *ACS Appl. Bio Mater.*, 2018, **1**, 1165–1173.
146 L. Tan, C. He, X. Chu, Y. Chu and Y. Ding, *Chem. Eng. J.*, 2020, **395**, 1385–8947.
147 Y. Huang, J. Qin, J. Wang, G. Yan, X. Wang and R. Tang, *Sci. China:Chem.*, 2018, **61**, 1447–1459.
148 M. H. Asfour and A. M. Mohsen, *J. Adv. Res.*, 2018, **9**, 17–26.
149 C. Zhang, M. Wang, J. Zhang, B. Zou and Y. Wang, *Colloids Surf., B*, 2023, **229**, 0927–7765.
150 S. Wang, W. Wu, Y. Liu, C. Wang, Q. Xu, Q. Lv, R. Huang and X. Li, *Drug Delivery*, 2022, **29**, 1951–1958.
151 G. G. Demissie, Y. C. Chen, S. Y. Ciou, S. H. Hsu, C. Y. Wang, C. C. Huang, H. T. Chang, Y. C. Lee and J. Y. Chang, *J. Colloid Interface Sci.*, 2025, **685**, 396–414.
152 Y. Wu, R. Guo, S. Wen, M. Shen, M. Zhu, J. Wang and X. Shi, *J. Mater. Chem. B*, 2014, **2**, 7410–7418.
153 L. Song, X. W. Chen, Y. Liu, H. Wang and J. Q. Li, *Int. J. Pharm.*, 2022, **619**, 0378–5173.
154 R. Dhivya, J. Ranjani, P. K. Bowen, J. Rajendhran, J. Mayandi and J. Annaraj, *Mater. Sci. Eng., C*, 2017, **80**, 59–68.
155 G. Chen, D. Li, J. Li, X. Cao, J. Wang, X. Shi and R. Guo, *New J. Chem.*, 2015, **39**, 2847–2855.
156 Y. Wu, K. Li, L. Kong, Y. Tang, G. Li, W. Jiang, M. Shen, R. Guo, Q. Zhao and X. Shi, *Bioconjugate Chem.*, 2020, **31**, 2404–2412.

157 F. Yang, X. Wen, Q. F. Ke, X. T. Xie and Y. P. Guo, *Mater. Sci. Eng., C*, 2018, **85**, 142–153.
158 M. Zhang, L. Lu, M. Ying, H. Ruan, X. Wang, H. Wang, Z. Chai, S. Wang, C. Zhan, J. Pan and W. Lu, *Mol. Pharm.*, 2018, **15**, 2437–2447.
159 D. Patiño-Ruiz, L. Marrugo, N. Reyes, M. Acevedo-Morantes and A. Herrera, *Int. J. Polym. Sci.*, 2020, **2020**, 1–10.
160 S. Huang, L. Deng, H. Zhang, L. Wang, Y. Zhang, Q. Lin, T. Gong, X. Sun, Z. Zhang and L. Zhang, *Nano Res.*, 2021, **15**, 728–737.
161 B. Zhou, B. Wu, J. Wang, Q. Qian, J. Wang, H. Xu, S. Yang, P. Feng, W. Chen, Y. Li, J. Jiang and B. Han, *Colloids Surf., B*, 2018, **163**, 284–290.
162 H. Iqbal, A. Razzaq, F. Liu, F. Zhang, J. Tao, T. Li, Y. Jiang, Z. Zhao, M. Qin, X. Lin, H. Ke, H. Chen and Y. Deng, *J. Controlled Release*, 2024, **372**, 829–845.
163 Y. Sun, S. Liu, Y. Gao, Y. Du, H. Cai, J. Zhang, Z. Wang, X. Yang, L. Hao and F. Yan, *ACS Appl. Nano Mater.*, 2021, **4**, 10556–10564.
164 J. Cheng, J. Li, Q. Yu, P. Li, J. Huang, J. Li, L. Guan, Z. Xu, J. Xiao and X. Duan, *J. Nanobiotechnol.*, 2024, **22**, 1477–3155.
165 M. Alikhani, M. Ramezani, K. Abnous, S. M. Taghdisi, S. Nekooei and M. Alibolandi, *J. Drug Delivery Sci. Technol.*, 2025, **103**, 1773–2247.
166 S. Raveendran, A. Giram, M. Elmi, S. Ray, C. Ireson, M. Alavijeh and I. N. Savina, *Biomedicines*, 2024, **12**, 2227–9059.
167 K. Bouzinab, H. S. Summers, M. F. G. Stevens, C. J. Moody, N. R. Thomas, P. Gershkovich, N. Weston, M. B. Ashford, T. D. Bradshaw and L. Turyanska, *ACS Appl. Mater. Interfaces*, 2020, **12**, 12609–12617.
168 L. Sun, M. Hou, L. Zhang, D. Qian, Q. Yang, Z. Xu, Y. Kang and P. Xue, *Nanomed. Nanotechnol. Biol. Med.*, 2019, **17**, 1–12.
169 X. J. Zhao, L. S. Li, P. W. Chen, D. Cheng, B. B. Liu and M. X. Zhao, *Mater. Chem. Phys.*, 2025, **343**, 131060.
170 T. Wu, Y. Shi, T. Yang, P. Zhao, Z. Yang and B. Yang, *RSC Adv.*, 2024, **14**, 9602–9608.
171 W. Song, J. Gong, Y. Wang, Y. Zhang, H. Zhang, W. Zhang, H. Zhang, X. Liu, T. Zhang, W. Yin, W. Yang and J. Nanopart, *Res*, 2016, **18**, 1572–896X.
172 E. Vélez-Peña, V. A. Jiménez, J. Manzo-Merino, V. Melin, D. Contreras, J. B. Alderete and C. H. Campos, *J. Drug Delivery Sci. Technol.*, 2025, **106**, 1773–2247.
173 L. Zhang, P. Zhang, Q. Zhao, Y. Zhang, L. Cao and Y. Luan, *J. Colloid Interface Sci.*, 2016, **464**, 126–136.
174 H. Zhang, B. Chen, H. Jiang, C. Wang and H. Wang, *Biomaterials*, 2011, **32**, 1906–1914.
175 Y. Chen, Z. Luo, C. Chen, M. Luo and L. Yuan, *Biotechnol. Biotechnol. Equip.*, 2021, **35**, 1492–1504.
176 H. Yang, Q. Zhang, L. Dai, Y. Wang, G. Zheng, X. Zhang, D. Zheng, X. Ji, Y. Sang and Z. Nie, *Adv. Healthcare Mater.*, 2024, **13**, 2192–2640.
177 Y. Zhou, K. Vinothini, F. Dou, Y. Jing, A. A. Chuturgoon, T. Arumugam and M. Rajan, *Arabian J. Chem.*, 2022, **15**, 1878–5352.
178 D. S. Randive, K. P. Shejawal, S. D. Bhinge, M. A. Bhutkar, N. R. Jadhav, S. B. Patil and S. J. Nadaf, *Future J. Pharm. Sci.*, 2023, **9**, 2314–7253.
179 B. Kargar, M. Fazeli, Z. Sobhani, S. Hosseinzadeh, A. Solhjoo and A. R. Akbarizadeh, *Sci. Rep.*, 2024, **14**, 2045–2322.
180 T. Zhang, Y. Wang, X. Ma, C. Hou, S. Lv, D. Jia, Y. Lu, P. Xue, Y. Kang and Z. Xu, *Biomater. Sci.*, 2020, **8**, 473–484.
181 W. Raj, K. Jerczynski, M. Rahimi, A. Przekora, K. Matyjaszewski and J. Pietrasik, *Mater. Sci. Eng., C*, 2021, **130**, 0928–4931.
182 F. Liu, D. Wang, M. Zhang, L. Ma, C. Y. Yu and H. Wei, *Acta Biomater.*, 2022, **144**, 15–31.
183 R. Sedghi, M. Gholami, A. Shaabani, M. Saber and H. Niknejad, *Eur. Polym. J.*, 2020, **123**, 14–3057.
184 R. Rehman, M. Rafiq, H. Shafi, A. H. Rather, R. S. Khan, S. N. Raza, S. u. Rather, S. Majeed, N. A. Khan and F. A. Sheikh, *Int. J. Pharm.*, 2025, **671**, 0378–5173.
185 A. R. Ahmady, A. Solouk, S. Saber-Samandari, S. Akbari, H. Ghanbari and B. E. Brycki, *J. Colloid Interface Sci.*, 2023, **638**, 616–628.
186 H. Kordbacheh, E. Bahmani, S. Bybordi, A. Rezaee, Z. Dehghanian, N. Ehsanfar, P. Goleij, F. SharifianJazi and M. Irani, *J. Drug Delivery Sci. Technol.*, 2024, **99**, 1773–2247.
187 U. Aggarwal, A. K. Goyal and G. Rath, *Mater. Sci. Eng., C*, 2017, **75**, 125–132.
188 M. Radmansouri, E. Bahmani, E. Sarikhani, K. Rahmani, F. Sharifianjazi and M. Irani, *Int. J. Biol. Macromol.*, 2018, **116**, 378–384.
189 P. Ye, R. Yusufu, Z. Guan, T. Chen, S. Li, Y. Feng, X. Zeng, J. Lu, M. Luo and F. Wei, *Pharmaceutics*, 2024, **16**, 1999–4923.
190 K. Zeng, Q. Xu, J. Ouyang, Y. Han, J. Sheng, M. Wen, W. Chen and Y. N. Liu, *ACS Appl. Mater. Interfaces*, 2019, **11**, 6840–6849.
191 N. Qiu, X. Yang, Y. Zhang, J. Zhang, J. Ji, Y. Zhang, X. Kong, Y. Xi, D. Liu, L. Ye and G. Zhai, *J. Nanobiotechnol.*, 2021, **19**, 1477–3155.
192 X. Ren, W. Liu, H. Zhou, J. Wei, C. Mu, Y. Wan, X. Yang, A. Nie, Z. Liu, X. Yang and Z. Luo, *Chem. Eng. J.*, 2022, **431**, 1385–8947.
193 G. Liu, J. Zou, Q. Tang, X. Yang, Y. Zhang, Q. Zhang, W. Huang, P. Chen, J. Shao and X. Dong, *ACS Appl. Mater. Interfaces*, 2017, **9**, 40077–40086.
194 H. J. Huang, S. Y. Huang, T. H. Wang, T. Y. Lin, N. C. Huang, O. Shih, U. S. Jeng, C. Y. Chu and W. H. Chiang, *Carbohydr. Polym.*, 2023, **302**, 144–8617.